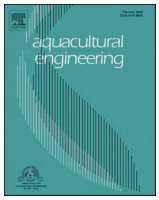
Aquacultural Engineering 98 (2022) 102255



Contents lists available at ScienceDirect

Aquacultural Engineering

journal homepage: www.elsevier.com/locate/aque





Experimental study on design and operational performance of solar-powered venturi aeration system developed for aquaculture – A semi-floating prototype

Mehmet Ali Dayıoğlu

Ankara University, Faculty of Agriculture, Department of Agricultural Machinery and Technologies Engineering, 06130, Ankara, Turkey

A R T I C L E I N F O

Keywords:
Venturi aeration
Dissolved oxygen
Solar energy
Aerator
Real-time monitoring
Operational performance

A B S T R A C T

Venturi-type injectors have been used usually due to the practical use and modular design that allows for quick configuration, ready-to-use, and low-cost solutions in the last years. This study aims to design a solar-powered venturi aeration system (SVAS) and determine its flow characteristics, standard, and real-time operational performance parameters. SVAS has a design providing the maximum vacuum and air velocity at air inlets and allowing for all technical measurements. Moreover, a solar-powered experimental apparatus having a weather station, a pool station, and a data logger station was constructed. Experiments were carried out using a plastic pool with a capacity of 4000 L, a diameter of 3 m and a depth of 0.75 m, four venturi injectors, and a submersible pump of 0.3 kW operated at the constant water flow regime of 4.1 m^3 h^{-1}. According to flow tests, the oxygen mass flow rates ranged from 2.77 to 2.84 kg h^{-1}. The specific energy consumption values are 263.2 kJ per cubic meter for water flow and 380 kJ per kg for oxygen transfer.

Standard performance experiments were repeated four times. The maximum overall oxygen mass transfer coefficient obtained during the experiments was 5.58 h^{-1}. The maximum values of standard oxygen transfer rate (SOTR), standard aeration efficiency (SAE), and standard oxygen transfer efficiency (SOTE) were 0.206 kgO_2 h^{-1}, 0.681 kgO_2 kWh^{-1}, and 7.32%, respectively. The pool conditions were simulated using de-oxygenation and mixing systems to determine the operational performance. For simulation experiments, six procedures and two processes were applied. Throughout operational experiments of four days, real-time dissolved oxygen levels fluctuated between 1.05 mg L^{-1} and 6.65 mg L^{-1}. The maximum performance values were 0.143 kgO_2 h^{-1} for the actual oxygen-transfer rate, 0.474 kgO_2 kWh^{-1} for aeration efficiency, and 5.1% for oxygen transfer efficiency.

1. Introduction

Aquaculture production has steadily augmented over a decade, ranking Turkey among the foremost aquaculture producers in the Mediterranean region. The total aquaculture production reached 273,400 tons in 2017, doubling the production in 2005. Rainbow trout culture was approximately 40% of the aquaculture production (FAO, 2019). Inland aquaculture in Turkey has been conducted in concrete ponds and net cages in dams, lakes, and reservoirs at small, medium, and high scales. However, there is no aerator because of the economic problems in most small-scale fish farms, where they are commonly far from national electricity power grids. Since the oxygen gained naturally is less than the oxygen lost in the aquatic ecosystem, insufficient aeration has caused fish deaths, low stocking, production losses, and quality losses.

The most vital parameters are the dissolved oxygen (DO) concentration and water temperature for all aquatic species. Those are interrelated, and a temperature change can cause more considerable changes in dissolved oxygen concentrations in ponds. As a common precept for most aquatic organisms, the best concentrations are 50% saturation in freshwater at sea level, so 5 mg L^{-1} at 15 °C and 4 mg L^{-1} at 26 °C (Boyd, 2015). For fish to reproduce and grow normally, the dissolved oxygen concentration range is generally 7–9 mg L^{-1} for most stream fish, including cold-water fish like trout and salmon, and 4–7 mg L^{-1} for warm water fish (Roy et al., 2021).

Generally, three methods can be used for artificial aeration or mechanical aeration: (1) surface aeration, (2) diffused aeration, and (3) gravity aeration (Roy et al., 2021). The common surface aerators are paddle-wheel type aeratorsthat rotate wheels to splash the water.

E-mail address: dayioglu@agri.ankara.edu.tr.

https://doi.org/10.1016/j.aquaeng.2022.102255
Received 17 October 2020; Received in revised form 28 March 2022; Accepted 6 April 2022
Available online 18 April 2022
0144-8609/© 2022 Elsevier B.V. All rights reserved.

Nomenclature

AAE (kg O_2·kWh^{-1}) Actual aeration efficiency
AOTE (%) Actual oxygen transfer efficiency
AOTR (kg O_2·h^{-1}) Actual oxygen transfer rate
C (mg L^{-1}) Dissolved oxygen concentration
C_0 (mg L^{-1}) Instantaneous dissolved oxygen concentration at time t = 0
C_s (mg L^{-1}) Saturation concentration of dissolved oxygen
C_s^{ℓ} (mg L^{-1}) Saturation concentration of dissolved oxygen at ℓ location
C_s* (mg L^{-1}) Saturation concentration of dissolved oxygen at standard condition
C_{s20} (mg L^{-1}) Saturation concentration of dissolved oxygen at 20 °C
C_t (mg L^{-1}) Instantaneous dissolved oxygen concentration at time t
f Mass fraction of oxygen in the air
F Fouling factor
i Number of venturi injector
I (A) Current
I_s (W m^{-2}) Solar irradiance
K_{La} (min^{-1}, h^{-1}) Overall oxygen mass transfer coefficient
K_{La20} (min^{-1}, h^{-1}) Overall oxygen mass transfer coefficient at 20 °C
m_{o2} (kg h^{-1}) Oxygen mass flow rate
P (W, kW) Power
P_b (kPa) Barometric pressure
P_g (bar) Pressure gage
P_{O2} (kWh kg^{-1}) Specific energy consumption for oxygen mass transfer
P_s (kPa) Standard atmospheric pressure
P_v (kPa) Vapor pressure
P_{vs} (kPa) Saturated vapor pressure
P_W (kWh m^{-3}) Specific energy consumption for water
RH (%) relative humidity
Q_a (m^3 h^{-1}) airflow rate
Q_w (m^3 h^{-1}) water flow rate
SAE (kg O_2·kWh^{-1}) standard aeration efficiency
SOTE (%) standard oxygen transfer efficiency
SOTR (kg O_2·h^{-1}) standard oxygen transfer rate
t (hh:mm:ss) time
T_a (°C) air temperature
T_w (°C) water temperature
T (K) absolute temperature
v_a (*m s^{-1}*) air velocity at inlet Venturi injector
v_w (*m s^{-1}*) wind speed
V (V) voltage
V_g (mmHg) vacuum gage
V_p (m^3) pool volume
W (kg kg^{-1} dry air) humidity ratio
α oxygen transfer correction factor
β oxygen solubility correction factor
ε (*m^3 m^{-3}*) Specific air transfer ratio
μ (m^3 kg^{-1} dry air) moist air specific volume
ρ_a (kg m^{-3}) density of air
τ (kg O_2 m^{-3}) specific oxygen transfer ratio
θ temperature correction factor

Abbr
ASCE American Society of Civil Engineers
CSC circular stepped cascade pump
DO dissolved oxygen concentration in water
OD Oxygen deficit
PAP propeller aspirator pump
PCSC pooled circular stepped cascade pump
PT perforated tray
PW paddle wheel
PS Percentage of saturation
SPW spiral aerator – modified paddle wheel
SVAS Solar - powered venturi aeration system
V venturi

Commonly, they consist of a frame, floats, motor, coupling, wheel, bearing, and speed reduction mechanism (Boyd, 1998; Peterson and Walker, 2002; Kumar et al., 2013a; Park et al., 2014; Brown et al., 2016; Roy et al., 2017, Brown and Tucker, 2014). The common types of diffused aerators are the propeller aspirator type, submersible type, air-jet type, and impeller type aerators; they consist of a rotating hollow pipe attached to the motor and the motor connected to the propeller (Kumar et al., 2010, 2013a; Jayraj et al., 2018). The common types of gravity aerators are the circular stepped cascade, pooled circular stepped cascade, and perforated pooled circular stepped cascade aerators, which are designed in circular steps uniformly distributing to fall from the upper step to subsequent next, water raised by a pump (Kumar et al., 2013b; Roy et al., 2020).

The venturi principle is a well-known technique used in water engineering. In the last decades, venturi type-bubble generatorshave been used primarily to produce fine bubbles, microbubbles, and nanobubbles in different areas, including aquaculture. These generators have taken considerable attention due to their simple structure, high efficiency, and low energy consumption (Mukhtar at al., 2010; Yin et al., 2015; Boyd and McNevin, 2020; Huang et al., 2020; Wang et al., 2020; Sakamatapan et al., 2021). The smaller the diameter of the bubbles in the water, the longer the residence time in the water, the more stable the phase interface, and the larger the specific surface area. Fujiwara et al. (2007) proposed a technique that used a converging-diverging nozzle to generate microbubbles and explained the effects of flow velocity at the throat on the bubble behavior. Vilaida et al. (2019) focused on an apparatus and its settings to find a suitable air-to-water ratio for the best microbubble generation for various venturi sizes of 3, 4, and 5 mm. Afisna et al. (2017) and Liew et al. (2020) studied porous-venturi microbubble generators and topics related to aeration efficiency, bubble distribution, and cavitation.

The air can be injected hydro-dynamically into the water in the form of bubbling flow with two-phase thanks to the structural specifications of venturi injectors. Each venturi injector has three main sections: (1) a converging cone section, (2) a throat section, and (3) a diverging cone section. According to the Bernoulli principle of conservation energy, the pressurized motive fluid flow at the inlet of its converging cone creates a perfect vacuum effect due to decreasing pressure at the throat. Tukimin et al. (2016) analyzed a venturi nozzle pressure drop and velocity discharge using Computational Fluid Dynamics (CFD). Gupta et al. (2016) investigated the flow characteristics of air-water flow in a venturi-channel located in a horizontal orientation. Yin et al. (2018) evaluated the DO variation in an air-water two-phase flow through a horizontal Venturi pipe with two holes, experimentally and numerically.

Venturi - type aerators have been used extensively as aeration methods in aquaculture. Baylar and Ozkan (2006) studied the geometric characteristics of venturi nozzle and factors affecting the air entrainment rate. Zhu et al. (2007) and Dong et al. (2012) studied different configurations of venturi air injectors connected either in series or parallel to achieve better aeration efficiencies for transferring oxygen into the water. Therrien et al. (2019) studied the performance of different design alternatives of a venturi-based aeration device consisting of venturi nozzles submerged in water and connected in parallel to a pump. Yadav et al. (2020) investigated the performance of the venturi

aeration system related to the air injection rate and aeration efficiency by using different throat length parameters with an increasing number of air holes to determine the aeration system suitable for aquaculture systems. Zhang et al. (2020) designed, produced, and optimized a new tube aeration device used in a circular fish tank to simultaneously realize the demands of the water and oxygen supplies. The effects of the structural parameters on the hydraulic efficiency and the oxygenation performance of the device were assessed in the study. Yadav et al. (2021) optimized using a non-dimensional technique the various geometrical parameters of the venturi aeration system, such as throat lengths, the number of air holes, and converging and diverging angles.

Furthermore, other studies that are conducted on aerators have usually concentrated on the aeration performance (Zhang et al., 2007; Kumar et al., 2013a, 2013b; Jayanthi et al., 2021; Yadav et al., 2021), water circulation and mixing (Lima et al., 2008; Jescovitch and Boyd, 2017; Itano et al., 2019), energy consumption (Brown et al., 2016; Boyd and McNevin, 2020), and renewable-powered aerators designed for fishponds (Applebaum et al., 2001; Cancino et al., 2004; Nookuea et al., 2016; Campana et al., 2019; Mahmudov et al., 2019; Nguyen et al., 2021; Ioakeimidis et al., 2013).

The performance indicators of aerators can be determined by the unsteady-state calculation method for measuring oxygen transfer in clean water defined by the American Society of Civil Engineers (ASCE). ASCE expresses according to standard conditions, which are zero DO concentrations, 20 °C water temperature, and atmospheric pressure at sea level for clean water. ASCE names the standard oxygen transfer rate (SOTR), standard aeration efficiency (SAE), and standard oxygen transfer efficiency (SOTE) (ASCE, 2007; Jiang and Stenstrom, 2012). The best suitable indicator for evaluating aeration efficiency is SAE (SOTR per power unit). The SOTR indicates the mass of oxygen that the aerator can introduce into a body of water per unit time under standard conditions. However, while proposed by ASCE, oxygen mass flow cannot be measured directly due to the structural features of most aerators during experiments, and SOTE cannot be calculated. SOTE estimates how much oxygen is transferred by a given aerator in clean water under the American Society of Civil Engineers' testing standards. The higher the percentage SOTE, the less air is needed. Bubble size is the single most significant factor in determining SOTE. The smaller the bubble, the higher the efficiency. The larger the bubble, the faster it rises. SOTE is not an energy efficiency calculation method, just of the oxygen transfer mechanism.

However, we would like to know what aerator performance is even in non-standard conditions. The actual performance of each aerator depends on field conditions in which the physical dynamics in fishponds, dams, and lakes are complex. The oxygen transfer rate is directly related to the oxygen deficit, water temperature, barometric pressure, and salinity. There is always a difference between standard and operational performances in the field. If given incomplete information related to on-field success in the catalogue, this situation can cause confusion and misunderstanding among the designer, equipment supplier, and fish farmer.

Each aquaculture pond has unique field conditions in terms of site elevation, temperature, the desired DO level, diffuser submergence depth, and different correction factors. Real-time monitoring plays an essential role in ensuring sustainable production in aquaculture. Operational performance 24/7 monitoring of aerators will be possible under actual culture conditions if the SAE of the aerator is known.

Even though the literature includes many studies on aerators used in aquaculture, relatively little attention has been paid to experimental studies on aerators with renewable energy using a broad systematic approach from design to operational performance. In this study, a solar-powered venturi aeration system (SVAS) is proposed as a specific design suitable for measuring the standard and operational performances to create sufficient and stable vacuum conditions at whole inlets of multiple venturi injectors. The different designs can be reconfigured thanks to no internal moving parts, mounting simplicity, and modular connection quickly. Water flow and airflow parameters can be measured easily. Meteorology and water conditions, as well as operational indicators, can be monitored in real-time.

The aim of this study is to design a solar-powered venturi aeration system, and to determine the characteristics and performance of a solar-powered venturi aerator, specifically: (1) the air and water flow characteristics of the configuration designed, (2) the SOTR, SAE, and SOTE performance parameters of the aerator, and (3) the operational performance of the aerator under simulated experimental conditions. The design of the appropriate solar power system is also discussed.

2. Materials and methods

This study analyzes systematically a solar-powered venturi aeration system (SVAS) based on sub-sections the following: (1) water and airflow model, (2) standard performance model, (3) operational performance model, (4) the description and implementation of SVAS, (5) experimental processes and procedures. SVAS is a new design enabling both developing a perfect vacuum at the air inlet of each venturi and allowing the measure of air velocity at the air intakes.

2.1. Water flow and airflow models

According to the experience acquired from pool experiments, the best design of SVAS was carried out directly connecting pipe fittings and venturi injectors on the discharge line of the pump without dividing flow. This design ensured the development of a perfect vacuum at the highest levels at the air intake points of all venturis. Fig. 1 shows the water flow and airflow models of SVAS, providing the gain of stable vacuum at maximum levels for each venturi.

The specific energy consumption (P_W) for motive fluid can be defined as follows, in kWh per cubic meter for water flow:

$$P_W = \left(\frac{P}{Q_w}\right) \tag{1}$$

Where Q_w is the water flow rate ($m^3\ h^{-1}$).

Power (P) consumed by the aerator is calculated by measuring current consumption (I) and voltage (V):

$$P = I \bullet V \quad \bullet 10^{-3} \tag{2}$$

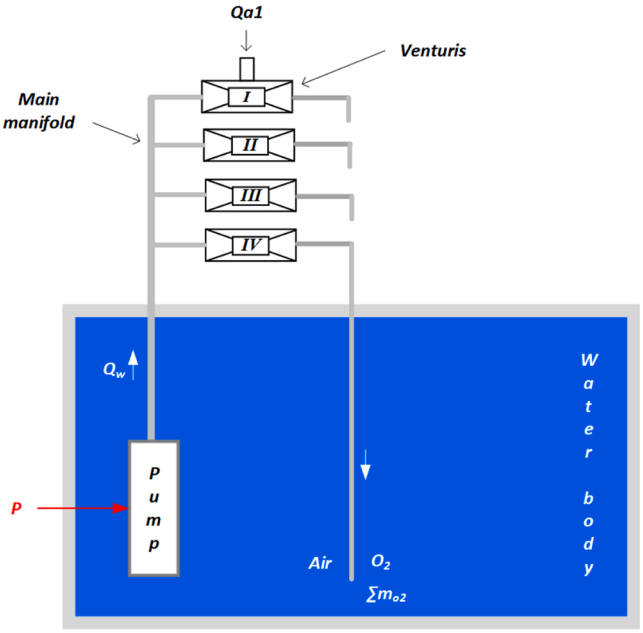


Fig. 1. Water flow and airflow models of the SVAS.

The specific air transfer ratio (ε) can be defined in Eq. (3):

$$\varepsilon = \frac{\sum Q_a}{Q_w} \tag{3}$$

Where Q_w is the water flow rate ($m^3\ h^{-1}$), $\sum Q_a$ is the total suction air flow rate ($m^3\ h^{-1}$).

The specific oxygen transfer ratio (τ) can be defined by dividing the total oxygen mass by to water flow rate as follows:

$$\tau = \frac{\sum m_{o2}}{Q_w} \tag{4}$$

The total oxygen mass flow rate ($\sum m_{o2}$) is calculated as follows:

$$\sum m_{O2} = \sum_{i=1}^{4} Q_a \times \rho_a \times f \tag{5}$$

Where i represents the number of Venturi injectors connected to SVAS (i = 4 for this study). Q_a is the airflow rate, ρ_a is the density of moist air, f is the mass fraction of oxygen in the air calculated based on molecular weights of oxygen and air ($f = 0.21 \times 32 \div 29 = 0.232$ kg O_2 per kg air).

The air density (ρ_a) equation is given as follows (ASHRAE, 2009):

$$\rho_a = \frac{1}{\mu} \times (1 + W) \tag{6}$$

where μ is the specific volume of moist air, in m^3 per kg dry air:

$$\mu = \frac{0.287042 \bullet T_a(1 + 1.607858 \bullet W)}{P_b} \tag{7}$$

where T_a is the absolute temperature of the air (K).

The humidity ratio (W) can be calculated as follows, in kg water vapor per kg dry air:

$$W = 0.621945 \frac{P_v}{P_b - P_v} \tag{8}$$

Where P_b is the barometric pressure, the water vapor pressure (P_v) was as follows:

$$P_v = P_{vs} \frac{RH}{100} \tag{9}$$

The saturated vapor pressure (P_{vs}) is given in Eq. (10) the following for the temperature range of 0–200 °C (ASHRAE, 2009):

$$\ln(P_{vs}) = \frac{-5800.2206}{T_a} + 1.3914993 - 4.8640239 \times 10^{-2} T_a + 4.1764768 \times 10^{-5} {T_a}^2 - 1.4452093 \times 10^{-8} {T_a}^3 + 6.5459673 \ln(T_a) \tag{10}$$

Where T_a is the absolute temperature of the air over liquid water.

The specific energy consumption (P_{O2}) for oxygen mass transfer can be defined as the following:

$$P_{o2} = \left(\frac{P}{\sum m_{o2}}\right) \tag{11}$$

Where power (P) and total oxygen mass flow rate ($\sum m_{o2}$) are given in Eq. (2) and Eq. (5), respectively.

2.2. Standard performance model

2.2.1. Overall oxygen transfer coefficient

Aeration is a mass transfer event between the gas and liquid interface in the form of both laminar flow and turbulent flow in water until a dynamic equilibrium is provided (Moulick et al., 2002).

The overall oxygen transfer coefficient K_{La} was measured using the unsteady-state method and a dissolved oxygen sensor with the following differential equation (Boyd, 2015):

$$\frac{dC}{dt} = K_L a(C_s - C) \tag{12}$$

$$K_L a = \frac{\ln(C_s - C_1) - \ln(C_s - C_2)}{t_2 - t_1} \tag{13}$$

Where C_s shows DO concentration at saturation t is time, and subscripts 1 and 2 show time 1 and time 2, respectively. The overall mass transfer coefficient (K_{La}) can be computed from the slope of the linear plot between *ln* (C_s-C) and time t, or with an analytical method.

Based on the Benson and Krause model given by (Jørgensen and Bendoricchio, 2001), the saturation DO concentration of water can be computed using the following formula for the water temperature between 273.15 K and 313.15 K, standard atmospheric pressure, and no salinity water:

$$lnC_s = -139.34411 + \left(\frac{1.575701 \times 10^5}{T_w}\right) - \left(\frac{6.6423080 \times 10^7}{{T_w}^2}\right) + \left(\frac{1.243800 \times 10^{10}}{{T_w}^3}\right) - \left(\frac{8.621949 \times 10^{11}}{{T_w}^4}\right) \tag{14}$$

For evaluation, standard K_{La20} values were calculated using the standard reference temperature (20 °C) defined according to the Arrhenius temperature relation given below:

$$K_L a_{20} = K_L a \bullet \theta^{20 - T_w} \tag{15}$$

Where T_w is water temperature (°C), θ is the temperature correction factor (1.024) for clean water (ASCE, 2007).

2.2.2. Standard oxygen transfer rate (SOTR)

Based on the (K_{La20}) coefficient determined for a specific aerator, the standard oxygen transfer rate (SOTR) is calculated as follows (Boyd, 2015):

$$SOTR = K_L a_{20} C_{s20} \bullet V_p \bullet \quad 10^{-3} \tag{16}$$

Where *SOTR* is the standard oxygen transfer rate, in kg O_2 per hour; K_{La20} is the overall oxygen mass transfer coefficient at 20 °C (h^{-1}); C_{s20} (9.0924-g m^{-3}) is the saturation DO concentration in freshwater at 101.325 kPa and 20 °C. V_p is the volume of water in the test pool (m^3); 10^{-3} kg g^{-1}.

2.2.3. Standard aeration efficiency (SAE)

The standard Aeration Efficiency (*SAE*) defines the measured kg oxygen transferred per kW per hour during operation (ASCE, 2007):

$$SAE = \frac{SOTR}{P} \tag{17}$$

2.2.4. Standard oxygen transfer efficiency (SOTE)

Standard oxygen transfer efficiency (*SOTE*) indicates how much oxygen is transferred as a percentage of the supplied oxygen to the water by the aerator (ASCE, 2007; Jiang and Stenstrom, 2012; Jenkins, 2014):

$$SOTE = \frac{SOTR}{\sum m_{O2}} \times 100 \quad (18)$$

2.3. Operational performance model

2.3.1. Oxygen deficit

One of the suitable indicators is the oxygen deficit (OD), defined as follows (Boyd, 2015; Lawson, 2002):

$$OD = C_s - C \quad (19)$$

The saturation concentration of DO at a specific location (ℓ) can be computed as functions of barometric pressure (P_b), standard atmospheric pressure (P_s =101.325 kPa), and water vapor pressure (P_v) (Haandel and van der Lubbe, 2012):

$$C_s^{\ell} = C_s\left(\frac{P_b - P_v}{P_s - P_v}\right) \quad (20)$$

Where P_v is calculated using the relative humidity of air (RH) in Eq. (9) and the saturated vapor pressure (P_{vs}) given in Eq. (10).

2.3.2. Percentage of saturation

The percentage of saturation concentration of the oxygen levels in the water is calculated from Eq. (21) (Lekang, 2013).

$$PS = \frac{C}{C_s} \times 100 \quad (21)$$

2.3.3. Actual performance calculations

Boyd et al. (2018) emphasized that the adjusting factors related to temperature, oxygen solubility, and transfer rate must be used to correct the differences between test conditions and actual operating conditions. By adapting definitions given by Boyd and Tucker (1998), Tchobanoglous et al. (2014), and Boyd et al. (2018), the following expression can be used to calculate the actual oxygen-transfer rate (AOTR) under field conditions:

$$AOTR = SOTR\left(\frac{\beta C_s^{\ell} - C_p}{C_s^*}\right)\theta^{t_w-20} \bullet \alpha \bullet F \quad = SOTR \bullet \eta_{OE} \quad (22)$$

Where $AOTR$ is the actual oxygen-transfer rate in kg of oxygen per hour. C_s^{ℓ} is the saturation concentration of DO at a specific location (ℓ). C_p is the DO concentration of water in a pool or fishpond water (mg L^{-1}). θ is the temperature correction factor. T_w is water temperature (°C). β *is* the oxygen solubility correction factor, ranging from 0.92 to 1.00 (mean = 0.98) for pond water (Shelton and Boyd, 1983). α is the oxygen transfer correction factor, between 0.90 and 1.00 for most pond waters (Shelton and Boyd, 1983). F is a fouling factor, $F = 1$ for surface aerator (Tchobanoglous et al., 2014). The C_s* value given in Eq. (22) equals to 9.0924 for clean tap water at 20 °C and 101.325 kPa, but this must be corrected for the existing salinity (Boyd et al., 2018). The depth effect was not considered in the calculation because the aeration depth was 0.5 m. Here, η_{OE} , which depends on the physical, biological, and chemical properties of the water source, can be named as a conversion factor or operational efficiency factor.

Similarly, the actual aeration efficiency (AAE = SAE·η_{OE}) and the actual oxygen transfer efficiency (AOTE = SOTE·η_{OE}) can be defined from SAE and SOTE.

2.4. Description and implementation

SVAS has a simple and modular design that allows quick configuration, handling ready-to-use, low-cost components more suitable for most aquaculture. Fig. 2 illustrates the schematic view of this design built as a semi-floating prototype. The prototype consists of components as follows: (1) A submersible pump, (2) a floating panel, (3) four-Venturi injectors, (4) pipes, (5) pipe fittings (pipe nipples, T- pipes, elbow pipe), (6) metal diffusers, (7) a pump controller, (8) a charge controller, (10) gel type batteries, (10) mounting frame, and (11) photovoltaic (PV) solar panels. Table 1 gives a detailed list of the components of the system.

2.4.1. Solar power subsystem

Fig. 3(a) shows Turkey and Ankara's solar energy potential map (GEPA). Fig. 3(b) and (c) show plots of monthly average sunshine duration and the optimum the tilt angle, respectively, relating to monthly average daily global solar radiation, respectively. Ankara has an average yearly global solar radiation of 1527.5 kWh m^{-2}, and the yearly-total sunshine duration is 2741 h (GEPA, 2016). Specifically, Ankara has annual total-global solar radiation levels ranging between 1500 and 1550 kWh m^{-2} (GEPA, 2016). The monthly average daily solar radiation coming on a horizontal surface is 1.47 kWh m^{-2} in December and 6.35 kWh m^{-2} in July. The monthly average sunshine duration is 3.35 h in December and 11.06 h in July, as shown in Since cases of oxygen deficiency are mostly experienced in August and September in fish farms close to Ankara province, these months were preferred for design. For the August and September months, according to Fig. 3(b and c), an optimum of the tilt angle can be taken as 24.5°, and

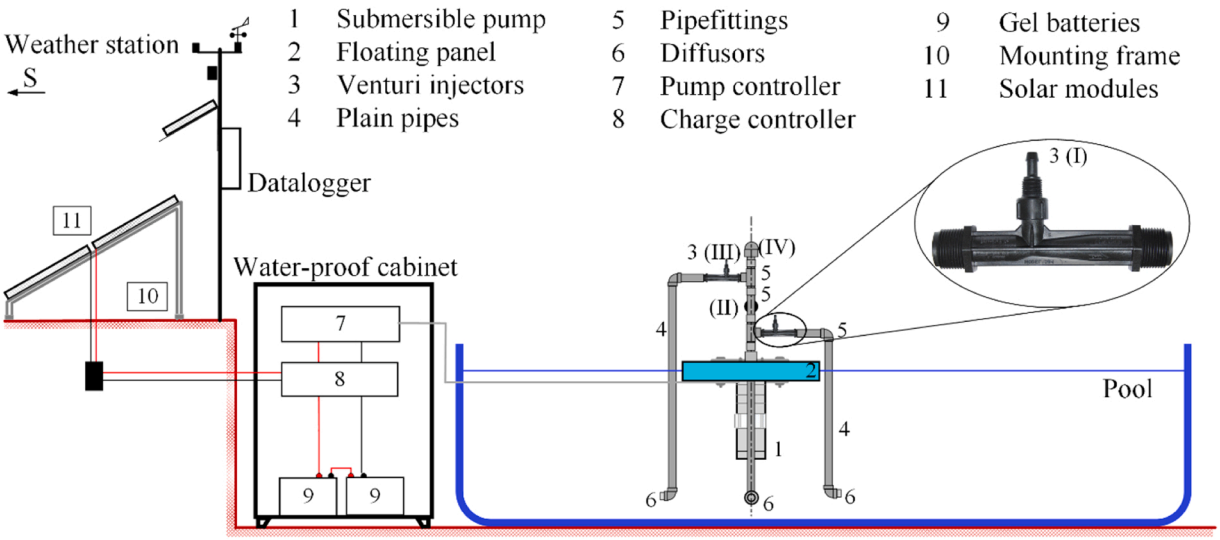


Fig. 2. Schematic view of the solar-powered venturi aeration system.

Table 1
Components of solar-powered venturi aeration system.

Devices	Manufacturer	Model	Specifications
Submersible pump	Lorentz, Germany	C-SJ5–8	Type: Centrifugal Motor: ECDRIVE 150-C DC brushless motor Nominal power: 300 W Max. flow rate: 4.6 m^3 h^{-1} Max. dynamic head: 20 m Efficiency: max. 92%
Pump controller	Lorentz, Germany	PS150	Power: max. 0.30 kW Input voltage: max. 50 V Optimum Voltage: > 17 V Nominal voltage (battery operation): 24 V Motor current: max. 18 A Efficiency: max. 98% Ambient temperature: − 30.50 °C Enclosure class: IP54
Venturi injectors	Netech, China	NT-A32235	Sizes: 32 × 25 × 32 mm Motive water flow rates: 3 – 10 m^3 h^{-1} Input pressures: 2 – 5 bar.
Solar panels	Zhejiang Heda Solar Technology Co., Ltd	HDS150M-36	Type: Monocrystalline Number: 2 (serial connection) Panel sizes: 1480 × 670×30 mm Panel weight: 13 kg Rated maximum power: 150 W_p Open circuit voltage (V_{oc}): 22.64 V Short circuit current (I_{sc}): 8.8 A Maximum power current: 8.01 A Maximum power voltage: 18.72 V Panel efficiency: 18.5% Total power output: 300 W_p Total panel area: 2 m^2
Batteries	Gold (Yalçın akü) Turkey	YGG12100.0	Type: Gel battery Weight: 31 kg Number: 2 (serial connection) Voltage: 12 V Total capacity: 100 Ah @ 24 V C - rate: 20
Charge controller	Juta, China	CM5024Z	Charge voltage: 24 V Current: 50 A Float voltage: 27.4 V Low voltage disconnection 21.4 V Low voltage reconnection: 25.2 V

the monthly average daily global solar radiation coming on a tilted surface is 5.8 kWh m^{-2}, and sunshine duration is 9.6 h.

Table 2 summarizes the design plan of the solar power subsystem used in SVAS. Monocrystalline type two solar panels were used where each has dimensions of 1480 × 670×30 mm, rated power of 150 W_p, and an efficiency of 18.5%. The total power output is 300 W, and the total solar panel area is 2 m^2. Gel type two batteries were used that each has a capacity of 100 Ah, a weight of 31 kg, and a total voltage output of 24 V. The daily maximum pump run time was taken as 5 h , and the total energy demand of 1500 Wh per day. The available energy capacity of the battery group is 2400 Wh (2 × 12 V @ 100 Ah). The daily energy output required of PV is 1765 Wh per day.

Fig. 4 shows photographs of the solar subsystem (a) the tilted solar panel and (b) the waterproof control cabinet, placed inside two batteries, a charge controller, and a pump controller. The solar panels were mounted on a galvanized tilt-adjustable perforated steel U-profiles (L = 2 m @ 40 × 40 × 40 mm and 30 × 30 × 30 mm), using bolts and nuts (M6–30 mm). Cross-sections of solar cables used for electrical connections were 4 mm^2 and 16 mm^2.

2.4.2. Aeration subsystem

The initial step in the development of SVAS is to create sufficient and stable vacuum conditions at all air inlets of venturi injectors (I-II-III-IV). The second step is to carry a suitable design so that water is not coming out of the air intake pipes of the venturi. This design was necessary since the wetting the risk of the sensor backflow occurred when the pump of SVAS was stopped. As an alternative solution, a check valve was used. It prevented water from coming out of water, but it caused vacuum loss at intake of venturis. Thanks to the experience obtained from pool experiments, the final design of SVAS was carried out by directly connecting pipe reducers, T- pipes, and venturi injectors on the discharge line of the pump without dividing the main motive flow. Fig. 5 shows the the final design implementation in that each venturi injector creates the perfect vacuum effect.

First, a pipe nipple (50 × 50 mm) was connected to pump's outlet of the pump, and then a T- pipe (50 × 50 × 50 mm). Second, a pipe nipple reducer (50 × 32 mm), a venturi injector-I (32 × 25 × 32 mm), an elbow pipe (32 × 32 mm), a delivery pipe (0.6 m × 32 mm), an elbow pipe (32 × 32 mm), and a metal diffuser (32 × 8 mm) are used. Third, other Venturi injectors were connected to the manifold. Finally, the remaining connections are finished with delivery pipes of 32 × 32 mm, and brass diffusers of 32 × 8 mm, as shown in Fig. 5 (see for I – II – III – IV).

However, a floating panel made from two insulation panels was used at sizes of 0.6 × 0.6 m at a thickness of 50 mm placed between two steel sheets to float the submersible pump. The pump was connected to the floating panel using its connection holes and steel brackets.

2.5. Experimental apparatus, setup, and planning

Experiments were performed in a plastic pool with a capacity of 4000 L having a diameter of 3 m, a height of 0.75 m shown in Fig. 6, between May 30, 2017, and August 30, 2017, at the Department of Agricultural Machinery and Technology Engineering, Ankara University, Faculty of Agriculture (39°57′41.27″ N, 32°51′59.90 E).

Fig. 7 illustrates the experimental apparatus used to measure water flow, airflow characteristics, and power consumption of the SVAS designed. The apparatus was composed of a pool station, weather station, and logging station. Table 3 gives the technical specifications of devices and sensors used in the apparatus.

The pool station consists of a DO probe (Sensorex Inc., DO1200/T), a water temperature sensor (Campbell Scientific Model 107), a water flow meter (Baylan multijet TK3C), a hot-wire anemometer (Lutron AM-4204), two certified manometers (Pakkens, MG063DRM1), a certified vacuum gauge (Pakkens, MG063DRP1-V14), a digital multimeter (Fluke 189), a DC clamp module (Fluke i410), a current clamp meter (Fluke 374 FC, a voltage module (Fluke v3001 FC), and a weather station combine temperature sensor (Texas Ins., LMT86), relative humidity sensor (Honeywell, HIH5031), solar radiation sensor (Apogee, SP110), barometric pressure sensor (Infineon, KP236N6165), an anemometer (Sparkfun, SEN-08942). The logging station comprises a data logger (Campbell Scientific, CR1000), a solar panel of 70 W, a charge controller, and a battery (12 V @ 26 Ah).

Fig. 8 shows the pool station (a) and the weather station (b), which were placed close to the pool station, the logger station (c), which was placed in a waterproof box, devices used for power measurements (d), and devices used for flow measurements (e).

The primary data set covers weather and pool variables measured simultaneously, such as air and water temperature, relative humidity, solar irradiance, barometric pressure, wind velocity, precipitation, and

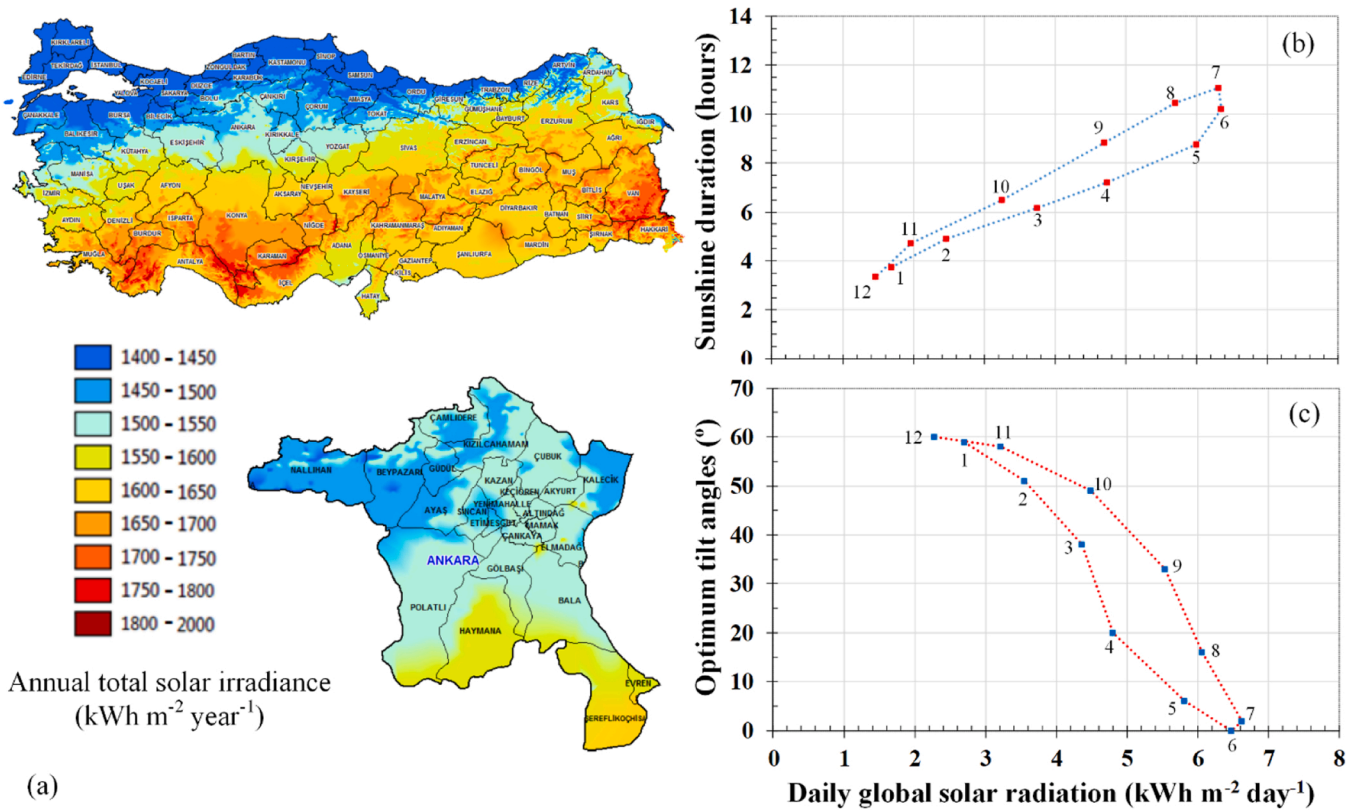


Fig. 3. (a) Annual total solar radiation potential maps for Turkey and Ankara (GEPA, 2016), (b) Monthly average daily global solar radiation on a horizontal surface and sunshine duration plot (adapted from GEPA, 2016 for Ankara), (c) Monthly average daily global solar radiation on a tilted surface and optimum tilt angles (adapted from Bakırcı, 2012 for Ankara).
(b) (adapted from GEPA, 2016 for Ankara) (c) (adapted from Bakırcı, 2012 for Ankara).

Table 2
Solar power subsystem worksheets.

Load	Battery sizing	PV panel sizing
Location: Ankara (39°57′41.27″ N, 32°51′59.90 E) Pump power: 300 W Battery voltage: 24 V Hours used per day: 5 h Total energy demand per day: 1500 Wh	Design temperature: 25 °C Battery voltage: 12 V Number of batteries: 2 Total battery capacity:100 Ah Energy capacity: 2400 Wh	Panel type: Monocrystalline Optimum design tilt: 24.5° Panel efficiency: 18.5% Design Month: August – September Required array output per day: 1765 Wh Number of panels: 2 Peak power output: 150 W Total peak power output: 300 W Total panel area: 2 m^2

dissolved oxygen concentration. The secondary data set includes parameters measured during flow and performance tests, such as power consumption (voltage and current), water flow rate, and air mass flow rate.

2.5.1. Experimental processes

- ***Pool setting process***- Clean-tap water was used in all tests performed during experiments. The aeration depth was 0.5 m, and the immersion depths of the DO probe and temperature sensor were 0.30 m.
- ***Power setting process***- All experiments were performed at a nominal power of 300 W and a nominal water flow rate. Before starting each experiment, by measuring the voltage and current simultaneously, the drawn power of the pump was adjusted using the rpm setting on the pump controller.
- ***Data acquisition process***- One-minute averages were recorded at sampling intervals of 5-second for weather data and 10-second for dissolved oxygen and water temperature data.
- ***Calibration process***- DO probes were calibrated using two data points, one in atmospheric air and one in a solution with zero dissolved oxygen.
- ***Deoxygenation process (*)***- This defines the process between almost 98% saturation and near 0% saturation while removing oxygen in the pool water, using sodium sulfite with chemical reaction given the following:

$$O_2 + 2Na_2SO_3 \xrightarrow{CoCl2\cdot 6H2O} 2Na_2SO_4$$

According to the stoichiometry of the above chemical equation, to deoxygenate water, sodium sulfite of 8 – 10 mg L^{-1} for each milligram per liter of DO is used, adding cobalt chloride of 0.05 – 0.1 mg L^{-1} cobalt as catalyst (Boyd, 1998). Water mixing is applied to accelerate chemical dissolution when applying the deoxygenation process.

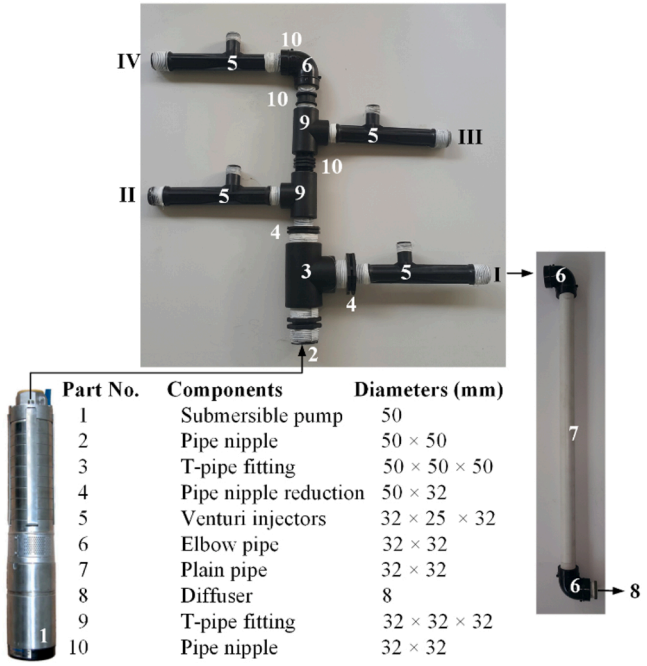
- ***Water mixing process (#)***- Mixing is applied to provide the uniform distribution of chemicals using an additional venturi injector immersed in water during standard performance tests and operational experiments.
- ***Reoxygenation process***- After running the aerator, this process covers changes from near 0% saturation to almost 98% saturation.

SVAS was operated using four venturi injectors at the following aeration modes:

- Continuous aeration mode for power setting and flow tests,
- Continuous aeration mode for standard performance tests,



Fig. 4. Photographs related to solar power subsystem (a) tilted PV solar panel, (b) control cabinet: 1) A charge controller, 2) Pump controller, 3) Gel-battery group.



Part No.	Components	Diameters (mm)
1	Submersible pump	50
2	Pipe nipple	50 × 50
3	T-pipe fitting	50 × 50 × 50
4	Pipe nipple reduction	50 × 32
5	Venturi injectors	32 × 25 × 32
6	Elbow pipe	32 × 32
7	Plain pipe	32 × 32
8	Diffuser	8
9	T-pipe fitting	32 × 32 × 32
10	Pipe nipple	32 × 32

Fig. 5. SVAS's components, sizes and final implementation.

- Intermittent aeration mode for operational tests (20 min on – 20 min off).

The experimental details are explained under the following sub-heads: Flow experiments, (3) Standard performance experiments, and (4) operational performance experiments.

2.5.2. Flow experiments

Flow experiments were performed between 30 May and 20 July 2017, using the experimental apparatus shown in Fig. 7. Before starting experiments, simultaneously taking voltage and current measurements, the pump was set up at a rated power of 300 W. During flow experiments, the pressure levels (P_g) at the inlet and outlet of the venturi injector were measured using two manometers connected to (1) and (2). A vacuum gage and a hot wire anemometer were connected to (3) point given in Fig. 7 to measure vacuum (V_g) levels and air velocity (v_a) at the air inlets of venturi injectors, respectively. SVAS's final configuration, consisting of single and multiple venturi injectors, was separately tested.



Fig. 6. Experiment pool and SVAS – semi-floating prototype.

After adding one-by-one-venturi injectors starting from the bottom injector, each experiment's the pressure and vacuum levels were measured using manometers and vacuum gage. Flow tests were repeated four times and recorded, taking one-minute averages of primary (weather and pool) data sampled during flow tests.

2.5.3. Standard performance experiments

Standard performance tests were carried out between 20 June and 10 August 2017, reconfiguring the experimental apparatus in depicted Fig. 7. The oxygen transfer rate was determined in clean water using the unsteady-state method described in standard ASCE/EWRI 2–06 (ASCE, 2007). Before starting each test, the test pool was refilled with 4000-L clean tap water, then power was set up to 0.3-kW, and DO concentrations were measured. The deoxygenation, reoxygenation, and mixing processes (see 2.5.1 section) were applied. The tests were repeated four times.

2.5.4. Operational performance experiments

The operational performance experiments planned as six procedures and two processes considering different scenarios were performed to simulate pool conditions between August 26 and 29, 2017. A mixing system with one venturi, a dosing system with one venturi, and electronic timer-controllers were use to conduct the simulations based on procedures.

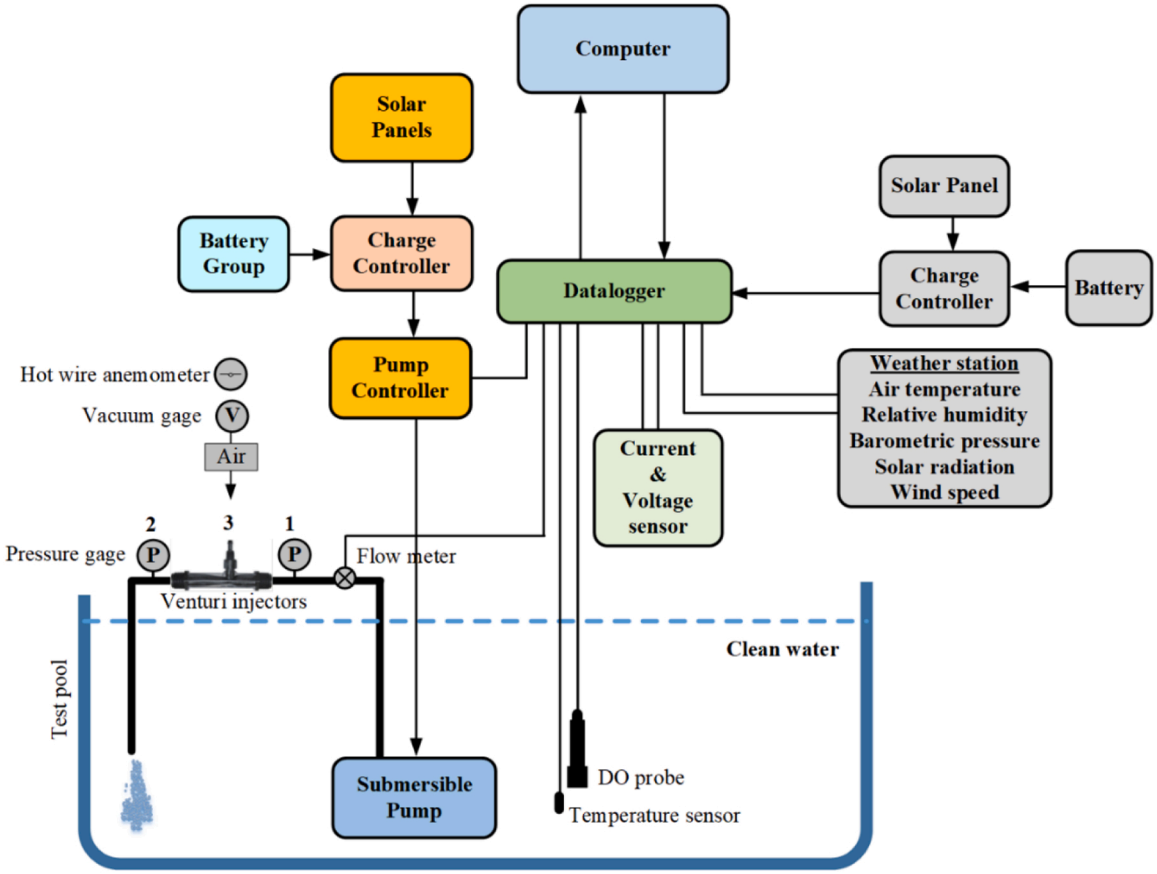


Fig. 7. Schematic drawing of the experimental apparatus.

Table 3
The devices used in the experimental system and their technical specifications.

Devices	*Manufacturer*	*Model*	*Specifications*	*Accuracy (Sensitivity)*
Datalogger	Campbell Scientific	CR1000	Power supply: 9.6–16 VDC Input voltage: ±5 V DC Analog inputs: 16 SE, 8 D Pulse counter: 2	±0.06%
Water temperature sensor	Campbell Scientific	Model 107	Analog, − 35° to + 100 °C	±0.4 °C
Dissolved oxygen probe	Sensorex Inc.	DO1200/T PTFE membrane	Analog, 0.1–20 mg L^{-1}	±0.1 mg L^{-1}
Wireless DC voltage module	Fluke	v3001 FC	Range: 0 – 60 V Resolution: 0.01 V	0.09%±3 digits
Current clamp module	Fluke	i410	Nominal current range 400 A, AC/DC	(1 mV/A)
Current clamp meter	Fluke	374 FC TRMS	DC current range: 0 – 600 A Resolution: 0.1 A DC voltage range: 0 – 600 V Resolution: 0.1 V	2%±5 digits 1%±5 digits
Digital multimeter	Fluke	189 TRMS	0–1000 V	±0.025%
Water flow meter	Baylan	Multijet TK3C	Pulse, 0–6.3 m^3 h^{-1}	±0.2%
Pressure gages	Pakkens	MG063DRM1	0–4 bar	CL 2.5
Vacuum gage	Pakkens	MG063DRP1-V14	-760–0 mmHg	CL 2.5
Hotwire anemometer	Lutron	AM-4204	Air velocity: 0–20 m s^{-1}	±1%
Anemometer	Sparkfun	SEN-08942	Pulse, 0–20 m s^{-1}	±1%
Solar radiation sensor	Apogee	SP110	Analog, 0–1750 W m^{-2}	(0.2 mV per W m^{-2})
Temperature sensor	Texas Ins.	LMT86	Analog, − 50 ° to + 150 °C	±0.4 °C
Relative humidity sensor	Honeywell	HIH5031	Analog, 0–100%	±3%
Barometric pressure sensor	Infineon	KP236N6165	Analog, 60–165 kPa	±1.0 kPa

The procedures and processes applied to the pool simulations during performance experiments are below:

Procedure A: no aeration – no mixing- The first is "Procedure A" in which neither aeration nor mixing is applied from 20:00 on August 26 to 08:00 on August 27, 2017.

Procedure B: intermittent aeration – water mixing – deoxygenation- The second is "Procedure B." were simultaneously applied the intermittent aeration and water mixing from 11:00 to 16:00 on August 27, 2017, the next deoxygenation was started at 21:30.

Procedure C: intermittent aeration – no mixing – deoxygenation – water mixing- "Procedure C" was performed on August 28, 2017; the intermittent aeration no mixing was applied from 06:00–10:00, after that deoxygenation at 10:00, and then the mixing process from 13:00–16:00.

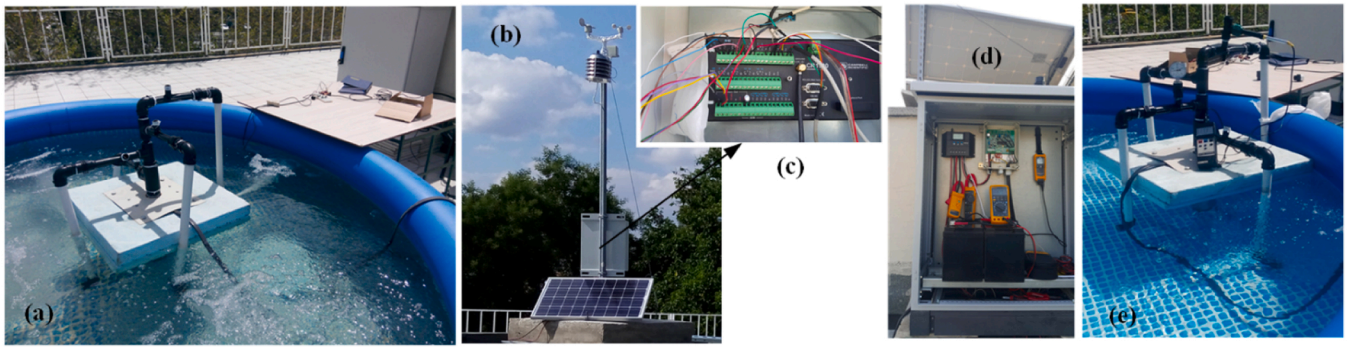


Fig. 8. Photographs of (a) pool station, (b) weather station, (c) datalogger, (d) power measurements (e) water flow – airflow measurements.

Procedure D: intermittent aeration – no mixing- In "Procedure D", which continued "Procedure C" on August 28, 2017, intermittent aeration without mixing was applied from 16:00–19:00, to be 20 min on and 20 min off. After that the deoxygenation process started at 23:30.

Procedure E: no aeration – water mixing - "Procedure E" was performed only water mixing, no aeration, from 00:00–05:00 on August 29, 2017.

Procedure F: intermittent aeration – water mixing- "Procedure F" was operated on both aeration and water mixing simultaneously starting at 11:00 on August 29, 2017, 20 min on and 20 min off until 16:00.

Deoxygenation process (*)- The deoxygenation was applied three times: (1) at 21:30 on August 27, 2017, (2) at 10:00 on August 28, 2017, (3) at 23:30 on August 28, 2017.

Water mixing process (#)-The water mixing was applied four times: (1) from 11:00–16:00 on August 27, 2017, (2) from 13:00–16:00 on August 28, 2017, (3) from 00:00–05:00 on August 29, 2017, and (4) from 11:00–16:00 on August 29, 2017.

3. Results

Flow experiments of SVAS were performed separately up four venturi injectors that are the final configuration, starting from a single venturi. Whole performance experiments covering standard and operational were applied using four venturis.

3.1. Flow characteristics

Table 4 gives a statistical summary of primary and secondary data measured during water flow and airflow experiments. During experiments performed between 30 May and 20 July 2017, average values of air and water temperature levels, relative humidity, barometric pressure, solar irradiance, and wind speed were 24.4 °C and 22.5 °C, 26.2%, 91.9 kPa, 665.9 W m^{-2}, and 4.86 m s^{-1}, respectively. When the submersible pump was operated at the rated power of 300 W, the power consumption that was consistent with an average voltage of 24.03 V and an average current of 12.48 A varied between 295 and 305 W (A = 299.8 W, SD =1.44 W), the water flow rate between 4.0 m^3 h^{-1} and 4.14 m^3 h^{-1} (A= 4.1 m^3 h^{-1}, SD = 0.01 m^3 h^{-1}). Throughout the experiments, the water flow rate has been kept constant.

The pressure values measured at (1) point for four Venturi injectors (I-II-III-IV) shown in Fig. 7 were 2.3 bar, 1.5 bar, 1.2 bar, and 1.0 bar, respectively. Although the pressure levels at water inlets of the venturis decreased, it was observed that vacuum levels (V_g = −700 mmHg) were unchanged at air inlets of venturi injectors (I-II-III-IV, see Fig. 7). Similarly, air velocity levels measured between 2.1 and 2.5 m s^{-1} (A = 2.25 m s^{-1}, SD = 0.132 m s^{-1}). These results meant that the air

Table 4
Statistical summary related to flow experiments of SVAS (30 May and 20 July 2017).

Primary data n = 348	**Min**	**Max**	**A**	**M**	**SD**			
Air temperature (°C)	17.48	28.96	24.42	24.67	3.022			
Water temperature (°C)	19.32	24.83	22.49	22.82	1.927			
Relative humidity (%)	18.05	43.42	26.19	25.91	5.280			
Barometric pressure (kPa)	91.6	92.1	91.9	91.9	0.149			
Solar irradiance (W m^{-2})	249.5	864.0	665.9	710.7	172.9			
Wind speed (m s^{-1})	0.625	9.653	4.86	4.75	1.767			
Secondary data n = 462								
Voltage (V)	23.67	24.38	24.03	24.06	0.109			
Current (I)	12.45	12.50	12.48	12.47	0.018			
Power (W)	295.2	304.8	299.8	299.9	1.440			
Water flow rate (m^3 h^{-1})	4.00	4.14	4.10	4.10	0.010			
VIS	***P_g[a] (bar)***	***P_g[b] (bar)***	***V_g[c] (mmHg)***	***Airflow rate Q_a[d] (m^3 h^{-1}) n *= 4***				
I	*2.3*	*0.1*	*-700*	2.37	2.71	2.54	2.54	0.146
II	*1.5*			2.37	2.83	2.63	2.66	0.196
III	*1.2*			2.37	2.49	2.43	2.43	0.069
IV	*1.0*			2.37	2.71	2.57	2.60	0.143
Total airflow $\sum Q_a$						10.17	10.23	–
Total oxygen mass flow $\sum m_o$ (kg O_2 h^{-1})						2.83	2.85	–

n – the number of samplings,
*n *– the number of experiments repeated, A – average, M – median, SD – standard deviation,*
VIS – Venturi injector sequence (see Fig. 1 and Fig. 4),
I… IV presents how many injectors are connected consecutively during experiments
[a] *shows pressure levels measured at (1) before venturi in Fig. 5 after adding* one by one venturi injectors,
[b] *shows pressure levels measured at (2) after venturi in Fig. 5 after adding* one by one venturi injectors,
[c] *shows the vacuum levels measured at (3) in Fig. 5 after adding* one by one venturi injectors,
[d] *shows airflow rate calculated from air velocity measured using hotwire anemometer*

Table 5
SVAS's flow characteristics and specific performance and specific energy consumption parameters.

Parameters	Results
Power consumption (P)	299.8 W
Water flow rate (Q_w)	4.1 $m^3\ h^{-1}$
Total airflow rate ($\sum Q_a$)	10.2 $m^3\ h^{-1}$
Total oxygen mass flow rate ($\sum m_{O2}$)	2.84 kg h^{-1}
The specific air transfer ratio (ε)	2.49 $m^3\ m^{-3}$
The specific oxygen transfer ratio (τ)	0.693 kg $O_2\ m^{-3}$
Specific energy consumption for water flow (P_W)	0.0731 kWh m^{-3} (263.2 kJ m^{-3})
Specific energy consumption for oxygen transfer (P_{O2})	0.1056 kWh kg^{-1} (380.0 kJ kg^{-1})

velocities could remain stable since there was no change at vacuum levels at all inlets of venturi injectors. After measuring air velocity, the airflow rates were calculated. By summing the airflow rates varying between 2.4 and 2.8 $m^3\ h^{-1}$ (A = 2.54 $m^3\ h^{-1}$, SD = 0.139 $m^3\ h^{-1}$), the total airflow rate was $\sum Q_a = 10.2\ m^3\ h^{-1}$. As a result, the total oxygen mass flow rate was $\sum m_o = 2.84\ kg\ h^{-1}$.

Table 5 gives the SVAS's flow characteristics and specific energy consumption values. When the submersible pump was operated with a flow rate of 4 m^3 per hour at a rated power of 300 W, SVAS could transfer 10.2 m^3 air per hour and 2.8 kg oxygen per hour into the water body. Specific parameters were also determined using flow characteristics obtained from experiments. The specific air transfer ratio was $\varepsilon = 2.49\ m^3$ airflow per cubic meter water flow, the specific oxygen transfer ratio $\tau = 0.693$ kg O_2 per cubic meter of water flow. The specific-energy consumption values were $P_W = 263.2$ kJ (= 0.073 kWh) per cubic meter water flow, $P_{O2} = 380$ kJ (= 0.106 kWh) per kg oxygen transfer.

3.2. Overall oxygen mass transfer coefficients

Once the deoxygenation procedure was started, it was seen that the DO concentration dropped sharply in a few minutes from 98% saturation (nearly 8 mg L^{-1}) to 2% saturation (0.15-mg L^{-1}). After turning on SVAS, when it runs at an average air flow rate of 10-$m^3\ h^{-1}$, reaching the saturation equilibrium point took 35–40 min.

Fig. 9 shows the natural logarithm plots drawn between oxygen deficit and time and trend lines, having high correlation coefficients (R^2= 0.995 – 0.998). The overall oxygen transfer coefficients (K_{La}) were determined from the slopes of trend lines (Eq. 13). Determined from four experiments applied on SVAS, using four venturis, K_{La} values were found as 0.0930, 0.0830, 0.0864, and 0.0708 min^{-1} (5.58, 4.98, 5.18, 4.25 h^{-1}), respectively. The best K_{La} coefficient was 5.58 h^{-1}. When the submersible pump was operated at the rated power of 300 W, the average water flow rate was 4.17 $m^3\ h^{-1}$, and the total airflow rate was

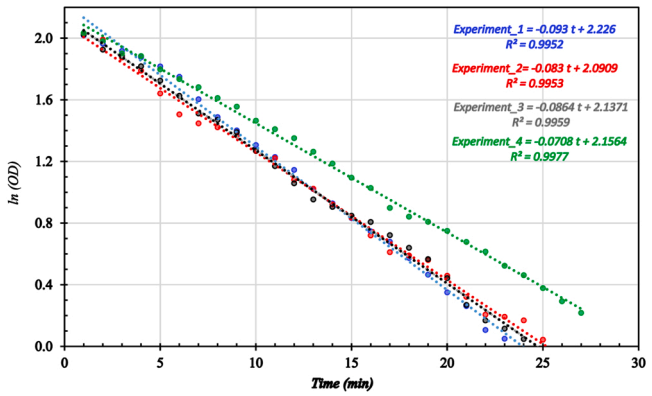


Fig. 9. Plots of natural logarithms of the oxygen deficit obtained from tests.

10.1 $m^3\ h^{-1}$. All values of $K_{La,}$ primary data, and descriptive statistics are presented in Table 6. Standard K_{La20} coefficients were 5.66, 4.90, 5.03, and 3.82 h^{-1} (A = 4.85 h^{-1}, M = 4.96 h^{-1} and SD = 0.765 h^{-1}), respectively.

3.3. Standard performance parameters

Determined from four experiments applied on SVAS, the standard performance parameters are given in Table 7. When operating at an average rated power of 0.3 kW, the average water flow rate was Q_w = 4.13 $m^3\ h^{-1}$, the total airflow rate was $\sum Q_a = 10.06\ m^3\ h^{-1}$and, the total-oxygen mass flow rate was $\sum m_o = 2.8\ kg\ h^{-1}$.

SOTR changed between 0.139 kg $O_2\ h^{-1}$ and 0.206 kg $O_2\ h^{-1}$ (A=0.177, M=0.181 and SD=0.0278 kg $O_2\ h^{-1}$). *SAE* values ranged from 0.463 kg O_2 kWh^{-1} to 0.681 kg O_2 kWh^{-1} (A=0.586, M=0.599 and SD=0.0906 kg O_2 kWh^{-1}). SOTE values were between 4.99% and 7.32 (A = 6.30%, M = 6.44%, SD = 0.9653%). In calculations related to performance, the highest values, averages, or medians of *SOTR*, *SAE*, and *SOTE* can be used to evaluate the success of SVAS.

3.4. Dissolved oxygen and environmental dynamics

Fig. 10 shows simultaneous plots for four-day measured at pool and weather stations between August 26 – 29, 2017. The fluctuations in the dissolved oxygen were similar to operations applied in the six scenarios defined in Section 2.5.4. However, during pool simulations, it was seen that there are always delays between action and reaction because the chemical process was slow. The meteorologic data covered air temperature (T_a), relative humidity (*RH*), solar radiation (I_s), barometric pressure (P_b), and wind speed (v_w) and pool data like water temperature (T_w), dissolved oxygen (DO) concentration. During aeration experiments for four days, the air temperature varied between 14.7–33.2 °C, the water temperature 18.8–26.4 °C, and relative humidity 12.3–84.3%. The sky was clear, there was no rain register, and the atmospheric pressure levels were almost stable between 91.1 kPa – 92.1 kPa. The maximum solar radiation and wind speed rose to 958 W m^{-2} and 11 m s^{-1}, respectively.

The fluctuations in the DO reflect the effects of simulations performed based on six scenarios (A, B, C, D, E, and F). Procedure A was applied from 20:00 on August 26–08:00 on August 27, 2017. Aeration and mixing processes are not performed. DO varied between 3.36 and 4.57 mg L^{-1} (A=4.05 mg L^{-1}, SD=0.226 mg L^{-1}). In Procedure B, which was simultaneously applied both intermittent aeration and water mixing from 11:00–16:00 on August 27, 2017, DO levels varied between 4.02 and 5.23 mg L^{-1} (A=4.48 mg L^{-1}, SD=0.217 mg L^{-1}). The deoxygenation process was applied at 21:30 when the DO concentration exceeded the level of 6.5 mg L^{-1}, and then DO levels decreased rapidly until 5 mg L^{-1}. In Procedure C, the intermittent aeration with no mixing, from 06:00–10:00 on August 28, 2017, DO varied between 4.49 and 6.48 mg L^{-1} (A=5.33 mg L^{-1}, SD=0.537 mg L^{-1}). As soon as the DO exceeded the 6.5 mg L^{-1}, after deoxygenation was applied at 10:00, , the mixing was applied between 13:00 and 16:00, DO levels decreased until 1.05 mg L^{-1}. When the intermittent aeration without mixing in Procedure D was applied from 16:00–19:00 on August 28, DO varied from 3.80 to 5.62 mg L^{-1} (A=5 mg L^{-1}, SD=0.555 mg L^{-1}). After deoxygenation at 23:30, mixing processes were applied between 00:00 and 05:00. In Procedure E, the water mixing process was performed only from 00:00–05:00 on August 29, 2017. DO varied between 3.38 and 5.43 mg L^{-1} (A=3.85 mg L^{-1}, SD=0.329 mg L^{-1}). In Procedure F, aeration and water mixing were applied simultaneously from 11:00 to 16:00 on August 29, 2017, DO levels varied between 3.76 and 6.47 mg L^{-1} (A=5.29 mg L^{-1}, SD=0.587 mg L^{-1}).

3.5. Operational performance results

Fig. 11 shows with simultaneous plots the actual performance results

Table 6
Summary of results related to overall oxygen mass transfer coefficients and primary data. (20 June and 10 August 2017).

*Experiments n * = 4*	*Overall oxygen mass transfer coefficients*			*Primary data[a] n = 242*					
	K_{La} (min^{-1})	K_{La} (h^{-1})	K_{La20} (h^{-1})	t_w (°C)	t_a (°C)	RH (%)	P_b (kPa)	I_s (Wm^{-2})	v_w ($m\,s^{-1}$)
1	0.0930	5.58	5.66	19.4	17.7	42.2	92.1	250.2	4.40
2	0.0830	4.98	4.90	20.7	21.1	29.5	91.7	566.4	2.62
3	0.0864	5.18	5.03	21.3	22.9	27.9	91.9	722.1	5.69
4	0.0708	4.25	3.82	24.5	27.3	19.3	91.6	153.7	3.89
A	**0.0833**	***5.00***	***4.85***	21.5	22.3	29.7	91.8	423.1	4.15
M	**0.0847**	***5.08***	***4.96***	20.9	22.0	28.7	91.8	408.3	4.14
SD	0.00931	*0.557*	*0.765*	2.167	3.998	9.446	0.222	266.1	1.271

*n * – the number of experiments repeated,*
n – number of samplings,
A – average, M – median, SD – standard deviation,
[a] *shows averages of data sampled during experiments.*

Table 7
Standard performance parameters determined by four experiments (20 June and 10 August 2017).

Experiments	*Operation conditions*				*Standard performance parameters*		
	P^a (W)	$Q_w{}^a$ ($m^3\,h^{-1}$)	$Q_a{}^b$ ($m^3\,h^{-1}$)	m_o ($kg\,h^{-1}$)	*SOTR* ($kg\,O_2\,h^{-1}$)	*SAE* ($kg\,O_2\,kWh^{-1}$)	*SOTE* (%)
1	302.1	4.17	10.10	2.81	0.2059	0.6814	7.32
2	298.3	4.00	9.95	2.77	0.1782	0.5974	6.43
3	304.8	4.20	10.20	2.84	0.1829	0.6002	6.44
4	300.2	4.15	10.00	2.78	0.1389	0.4628	4.99
A	301.4	4.13	10.06	2.80	***0.1765***	***0.5855***	***6.30***
M	301.2	4.16	10.05	2.80	***0.1806***	***0.5988***	***6.44***
SD	2.774	0.0891	0.1109	0.0309	0.0278	0.0906	0.9653

A - average, M – median, SD – standard deviation.
[a] *shows averages of data sampled during experiments,*
[b] *shows airflow rates calculated from air velocity measured using hotwire anemometer*

calculated for four-day between August 26 – 29, 2017. The performance parameters covered the oxygen deficit (OD), percentage of saturation (PS), actual oxygen-transfer rate (AOTR), actual aeration efficiency (AAE), and actual oxygen transfer efficiency (AOTE). The effects of experimental scenarios (A, B, C, D, E, and F) like in Fig. 10 are also seen in Fig. 11, as the dissolved oxygen concentration functions. Furthermore, daily descriptive statistics of scenarios applied during operational experiments are summarized in Table 8.

AOTR, AAE, and AOTE were determined from the medians of SOTR (180.6-g $O_2\,h^{-1}$), SAE (598.8- g $O_2\,kWh^{-1}$), and SOTE (6.44%). For A-B-C-D-E and F procedures, OD values varied between 3.24 and 5.08, 2.22 – 4.08, 1.3 – 6.2, 1.64 – 3.45, 2.28 – 4.54, and 0.86 – 4.02 mg L^{-1}, respectively. The maximum PS values were 58.5, 70.2, 83.6, 77.4, 70.4, 88.3%, respectively. In Procedure A, aeration and mixing processes were not performed between 20:00 on August 26 and 08:00 on August 27, 2017. Procedure E was applied between 00:00 and 05:00 on August 29, 2017; the aeration was not operated, the water was mixed only. The maximum AOTR values calculated were 82.4, 143, 79.6, and 85.1 g O_2 h^{-1} for B, C, D and F- procedures. For the same procedures, the maximum AAE values were 273.2, 474.2, 264, and 282 g O_2 kWh^{-1}, respectively. The maximum AOTE values were 2.94% for B, 5.1% for C, 2.84% for D, and 3% for F. Moreover, the highest SOTE obtained during standard tests was 7.32%. As expected, the operational performance values of an aerator are always lower than the specified standard performance values.

4. Discussion

SVAS occurs in two parts: The first part is the solar subsystem having a PV panel of 300 W, a solar charge controller, and a battery group of 24 V @ 100 Ah battery. The optimum tilt angle of the PV panels was adjusted to 24.5° by taking the mean of the optimum values determined for August and September. The second part is the aeration system with a submersible pump power of 0.3 kW, a pump controller, four venturi, and pipe fittings. The analysis of SVAS design was carried out in three steps:

The first analysis determines the flow characteristics and the specific power consumption. The trials showed that the pressure levels decreased from 2.3 bar for only one injector to 1.0 bar for four injectors measured at the pump's outlet . However, the stable vacuum effect (−700 mmHg) occurred at air inlets of all Venturi injectors, and air velocity values (v_a = 2.1–2.5 m s^{-1}) observed no change. These findings have strategic importance for design. Because knowing the hydrodynamic behavior of each modular connection added to the system provided a few advantages. Thus, it was determined how much oxygen from all injectors to the water, $\sum m_{o2}$ = 2.84 kg h^{-1}, was transferred with the SVAS of nominal power.

The second analysis is the overall oxygen mass transfer coefficients (K_{La}) to determine the oxygen transfer capability of SVAS. K_{La} coefficients (5.58, 4.98, 5.18, 4.25 h^{-1}) were obtained by taking absolute values of slopes using the linear trend lines with high correlation. Standard K_{La20} coefficients (5.66, 4.90, 5.03, and 3.82 h^{-1}) calculated using temperature corrected were found with a 4.85 h^{-1} average, a 4.96 h^{-1} median, and a 0.765 h^{-1} standard deviation. The results of this study are consistent with those of Boyd et al. (2018), who found that K_{La} coefficients at a water temperature of 25 °C were 5.38 h^{-1}, using a 7.5-kW aerator. However, it is seen that the powers installed of those are very different from each other. For Dong et al. (2012)'s venturi type aerators of 1.5 kW, K_{La} coefficients were partly coherent with changing between 3.31 h^{-1} and 12.92 h^{-1}; Kumar et al. (2014)'s K_{La} was 1.53 h^{-1} for the propeller-aspirated pump of 0.36 kW. Hence, it can be highlighted that the determination of the K_{La} coefficients depends on the hydrodynamics, installed power, experiment conditions, and the shape and structure of the system design.

SVAS's standard performance parameters were discussed in the overall evaluation and comparison with previous studies. Looking at the best SOTR and SAE values determined during the experiments, we understand that SVAS can oxygenate as much with 0.206 kg O_2 per hour and 0.687 kg O_2 per kWh the clean water in a particular volume,

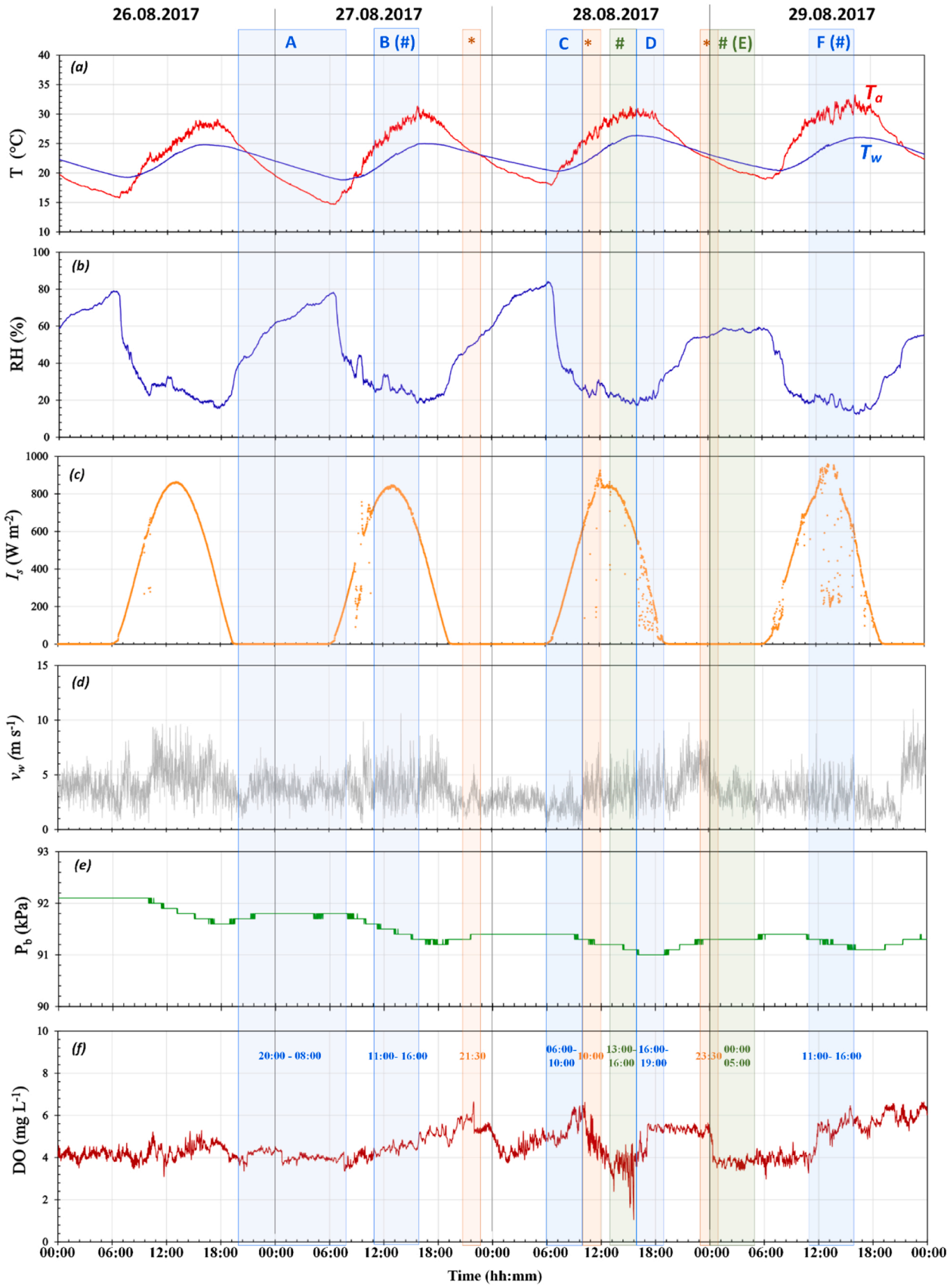


Fig. 10. Daily variations in primary data measured during operational experiments.

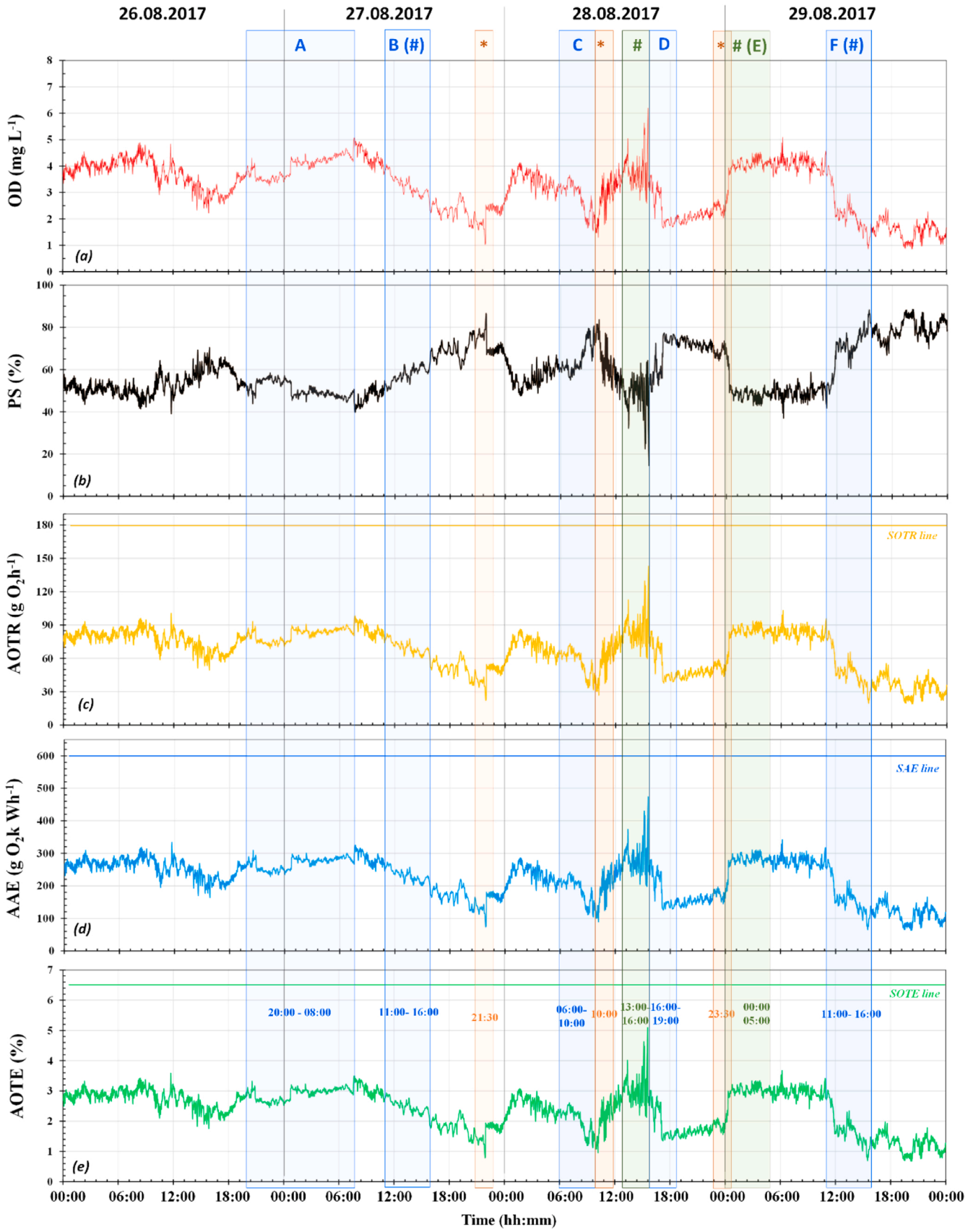


Fig. 11. Daily variations of operational performance parameters.

Table 8
Descriptive statistics determined for six procedures applied during operational experiments.

		DO	OD	PS	AOTR	AAE	AOTE
A no aeration no mixing	*Min.*	3.357	3.244	39.80	–	–	–
	Max.	4.566	5.077	58.46	–	–	–
	A	4.046	4.016	50.27	–	–	–
	SD	0.226	0.397	3.710	–	–	–
B +(#)	*Min.*	4.025	2.224	49.68	49.67	164.69	1.771
	Max.	5.229	4.076	70.16	82.39	273.17	2.938
	A	4.476	3.258	57.96	69.42	230.17	2.475
	SD	0.217	0.375	3.913	6.168	20.45	0.220
C +(/#)*	*Min.*	1.054	1.295	14.53	26.81	88.89	0.956
	Max.	6.624	6.200	83.64	143.03	474.23	5.100
	A	4.608	3.149	59.11	67.51	223.85	2.407
	SD	0.963	0.742	10.77	18.25	60.51	0.651
D no mixing	*Min.*	3.796	1.639	52.37	37.73	125.09	1.345
	Max.	5.618	3.453	77.42	79.61	263.96	2.839
	A	5.009	2.260	68.90	51.95	172.26	1.853
	SD	0.555	0.540	7.505	12.58	41.70	0.449
E no aeration only mixing	*Min.*	3.382	2.280	42.81	–	–	–
	Max.	5.425	4.535	70.41	–	–	–
	A	3.858	3.997	49.13	–	–	–
	SD	0.329	0.369	4.469	–	–	–
F +(#)	*Min.*	3.760	0.859	48.31	19.57	64.89	0.698
	Max.	6.465	4.024	88.27	85.07	282.05	3.033
	A	5.291	2.217	70.62	48.71	161.49	1.737
	SD	0.587	0.716	8.90	14.52	48.16	0.518

Table 9
Comparisons of the SOTR and SAE values obtained for SVAS and other aeration devices.

Line number	Aerator type	Power (kW)	SOTR (kg O_2 h^{-1})	SAE (kg O_2 kWh^{-1})	References
1	IM	0.400	0.200	0.490	Zhang et al. (2007)
2	IM	1.100	0.420	0.350	
3	IM	0.400	0.150	0.360	
4	IM & DA	2.200	0.210	0.100	
5	IM & DA	3.700	2.660	0.680	
6	IM & DA	4.800	2.930	0.570	
7	V	1.500	0.100	0.070	Zhu et al. (2007)
8	V	1.500	0.220	0.140	
9	PAP	0.360	0.150	0.420	Kumar et al. (2010)
10	V	1.500	0.306	0.204	Dong et al. (2012)
11	PCSC	0.186	0.161	0.867	Kumar et al. (2013a, 2013b)
12	CSC	0.186	0.135	0.726	
13	PW	0.746	2.600	3.485	
14	PW	1.492	5.000	3.351	
15	PAP	1.492	0.454	0.304	
16	PAP	0.400	0.112	0.280	Kumar et al. (2014)
17	CSC	0.160	0.135	0.844	
18	V	0.300	0.183	0.610	Dayıoğlu (2015)
19	V	0.300	0.201	0.670	
20	PT	0.250	0.025	0.100	Eltawil and Elsbaay (2016)
21	V	0.150	0.144	0.960	Gebremedhen (2016)
22	V	0.300	0.197	0.660	
23	SPW	1.490	1.490	1.000	Roy et al. (2017)
24	PW	7.500	8.900	1.110	Boyd et al. (2018)
25	V	0.180	0.039	0.217	Therrien et al. (2019)
26	V	0.150	0.025	0.167	
27	V	–	0.0216	0.611	Yadav et al. (2021)
28	V	0.300	0.139 – 0.206	0.463 – 0.687	This study

V – Venturi, PAP– propeller aspirator pump, PCSC – pooled circular stepped cascade pump,
CSC – circular stepped cascade pump, PW – paddlewheel, PT – perforated tray, SPW – spiral aerator-modified paddle wheel,
IM – impeller mixing, IM & DA – impeller mixing, and diffused air.

respectively.

Under similar conditions, SAE values can be used as a critical indicator for evaluating the performance of aerators. If knowing the SAE of the aerator, it is possible to estimate its oxygen-transfer rates under actual culture conditions. The standard conditions differ from actual field conditions.

Table 9 compares the SOTR and SAE values across previous literature and SVAS results. The different types of aerators are given with the following abbreviations: IM: Impeller mixing, IM & DA: Impeller mixing and diffused air, V: Venturi, PAP: propeller aspirator pump, PCSC: pooled circular stepped cascade pump, PT: perforated tray, CSC: circular stepped cascade pump, PW: paddlewheel, SPW: spiral aerator – modified paddle wheel. Most aerators employed in aquaculture have higher installed powers, ranging from 2.2 to 7.5 kW (Zhang et al., 2007; Kumar et al., 2013a; Roy et al., 2017; Boyd et al., 2018).

Zhang et al. (2007) and Dong et al. (2012) reported that SOTRs varied from 0.15 to 2.93 kg O_2 h^{-1}, and SAEs from 0.10 to 0.68 kg O_2 kWh^{-1} for impeller-diffused air type aerators at powers between 0.4 kW and 4.8 kW. Kumar et al. (2010) found best SOTR = 0.15 kg O_2 h^{-1} and SAE = 0.42 kg O_2 kWh^{-1} for a 0.14-m submergence depth, a 2840-rpm rotational speed, and at the positional angle of 75° of the propeller shaft. According to Dong et al. (2012), SOTR and SAE values varied from 0.141 to 0.306 kg O_2 h^{-1} and 0.094–0.204 kg O_2 kWh^{-1} for a Venturi type aerator, respectively. Standard performance results (SOTR and SAE) of Gebremedhen (2016) ranged from 0.144 to 197 kg O_2 h^{-1} and from 0.657 to 0.960 kg O_2 kWh^{-1} for a Venturi type aerator. Roy et al. (2017) reported SAE = 1.0 kg O_2 kWh^{-1} for a 1.5 kW spiral aerator-paddle wheel modified. Therrien et al. (2019) stated that SOTR values were between 0.025 and 0.039 kg O_2 h^{-1} and that SAE values were between 0.167 and 0.217 kg O_2 kWh^{-1}, respectively, for two Venturi type aerators having a 150 W and 180 W-rated power. Yadav et al. (2021) reported that SOTR= 0.0216 kg O_2 h^{-1} and SAE = 0.611 kg O_2 kWh^{-1} for venturi type aerator. Although the rated power of the pump is 1.49 kW, it is not specified whether the nominal power of the pump used in this study is used in the calculation of SAE.

SVAS' SOTR and SAE parameters were better than those of most aerators given in Table 9 used in aquaculture, although its installed power is smaller than in previous studies. To make meaningful comparisons among these studies, differences in experimental conditions must know. In terms of experiments, it is necessary to define the trial conditions affecting the performance, such as the volume of the tank where the tests are carried out and the installed aerator power, to make a correct evaluation.

While SAE is an indicator related to energy efficiency, SOTE is an indicator that shows how efficiently transferred the oxygen inside the form of the bubble is into the water. Since bubble size is an indicator used in defining SOTE, the smaller the bubble size means the higher the efficiency. Therefore, SOTE has commonly used to determine how much air it requires to provide the kilograms of oxygen needed for aerated fishponds. Looking at the best SOTE values obtained during the experiments, we understand that SVAS can transfer as much as 7.32%. Considering the values of only SOTE or SAE, there are several drawbacks in making comparisons of various aerators because of different trial conditions during tests. A fish farmer should never purchase an aerator without certified independent lab results to verify the manufacturer's performance indicators. Aerators tested in the same lab under the same conditions must be preferred.

The third analysis is the operational capability of SVAS based on pool simulations. Short-term experiments were carried out by applying six procedures in four days. Real-time primary data were monitored to analyze performance. Findings showed that given similar responses to fishpond conditions of pool simulations performed to create DO fluctuations in pool conditions. Although delays always occur between action and reaction during experiments, we can monitor the effects of procedures looking at DO fluctuations and standard deviations (SD) .

Fig. 12 shows as bar graphs four-day statistics of DO, OD, and PS on

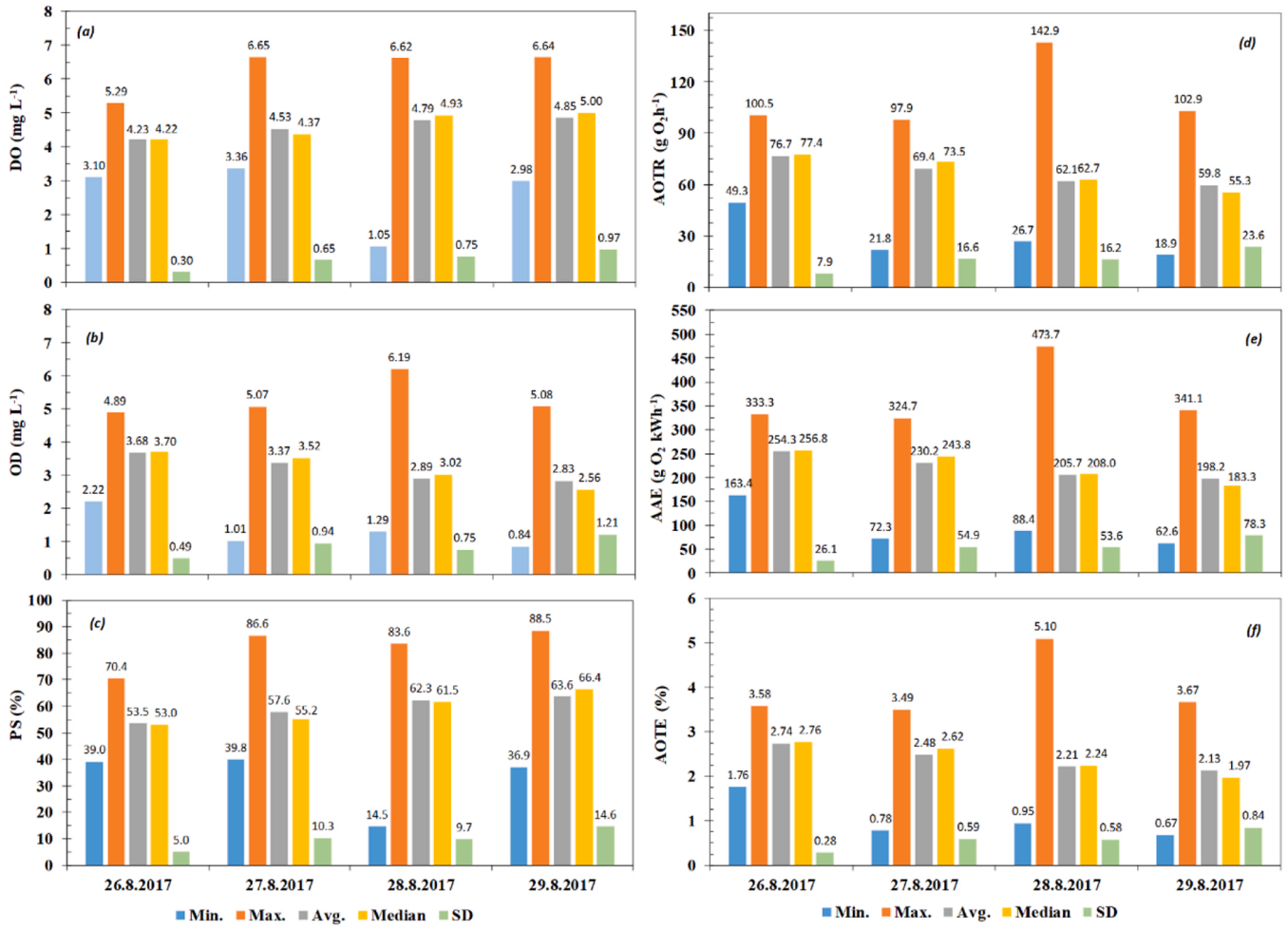


Fig. 12. Daily descriptive statistics related to the operational performance values, (a) Dissolved oxygen, (b) Oxygen deficit, (c) Percentage saturation, (d) Actual oxygen transfer rate, (e) Actual aeration efficiency and (f) Actual oxygen transfer efficiency.

the left side and those of AOTR, AAE, and AOTE on the right side, related to the operational performances given in the Results section.

As seen, the oxygen deficit directly affected system performance. The time graphs of dissolved oxygen and oxygen deficit are symmetric, ranged between 1.05 mg L^{-1} and 6.65 mg L^{-1} whereas ODs were between 0.841 mg L^{-1} and 6.19 mg L^{-1} (A = 3.19 mg L^{-1}, M = 3.42 mg L^{-1}, SD =0.954 mg L^{-1}). On the other hand, PS ranged from 14.5% to 88.6%, with an average of 59.3% (SD = 11.2%). The highest AOTR, AAE and AOTE values were 142.9 g O_2 h^{-1} (A = 67.0, M = 72.6, SD = 18.2), 473.7 g O_2 kWh^{-1} (A = 222.1, M = 240.6, SD = 60.5), 5.1% (A = 2.4, M = 2.6, SD = 0.65), respectively. Jescovitch and Boyd (2017), Park and Yang (2017), and Itano et al. (2019) highlighted that the water mixing and water circulation process directly affected the fluctuation of DO in water.

As expected, the water temperature significantly affected the system performance. As temperature increases, the saturated DO concentration decreases.

Consequently, during experiments, C_s values varied from 7.23 at 26.4℃ to 8.42 mg L^{-1} at 18.9℃. And the performance of the aerator was discussed using scatter plots to evaluate interactions.

The oxygen transfer rate can be estimated using the oxygen deficit, or dissolved oxygen data. If known as real-time DOs or ODs, real-time operational performance values of SVAS can be determined. Fig. 13(a) shows daily scatter plots between DO versus water temperature, defined with red, blue, green, and black colors on 26, 27, 28, and 29 August, respectively. Thus, analysis results can be extracted at different time scales such as hourly, day, night, daily, weekly, monthly, etc., similar to the four-day analysis results.

Fig. 13(b-c) shows the relationships between dissolved oxygen and oxygen deficit versus daily operational efficiency. DO and OD trend lines obtained from experiments are shown with the dashed orange and gray lines in Fig. 13(b) and (c), respectively. The operational efficiencies are defined as percentage using the following equations for both dissolved oxygen and oxygen deficit:

$$\eta_{OE} = -13.239 \bullet \quad DO + 97.989 (R^2 = 0.9724) \tag{23}$$

$$\eta_{OE} = 10.471 \bullet \quad OD + 3.6549 (R^2 = 0.9785) \tag{24}$$

These linear equations can be used for practical calculations and comparisons. SVAS operates at an efficiency equal to roughly 71.5, 58.3, and 45.0% of their SAEs at DO concentrations of 2, 3, and 4 mg L^{-1}. These findings are consistent with Boyd et al. (2018)'s, who reported as 70%, 60%, and 40%– 50% for the same DO concentrations. Considering the oxygen deficit levels of 3, 4, and 5 mg L^{-1}, aeration efficiencies will be 35%, 46%, and 56%, respectively.

Tests and experiments have shown the applicability of prototype SVAS developed for fish farms. These findings are valuable in identifying how SVAS has responded to a particular oxygen deficit or biological oxygen demand in different fishponds during aeration.

5. Conclusion

SVAS was designed to develop a system consuming less power per cubic meter of water flow to transfer more oxygen into the water, using

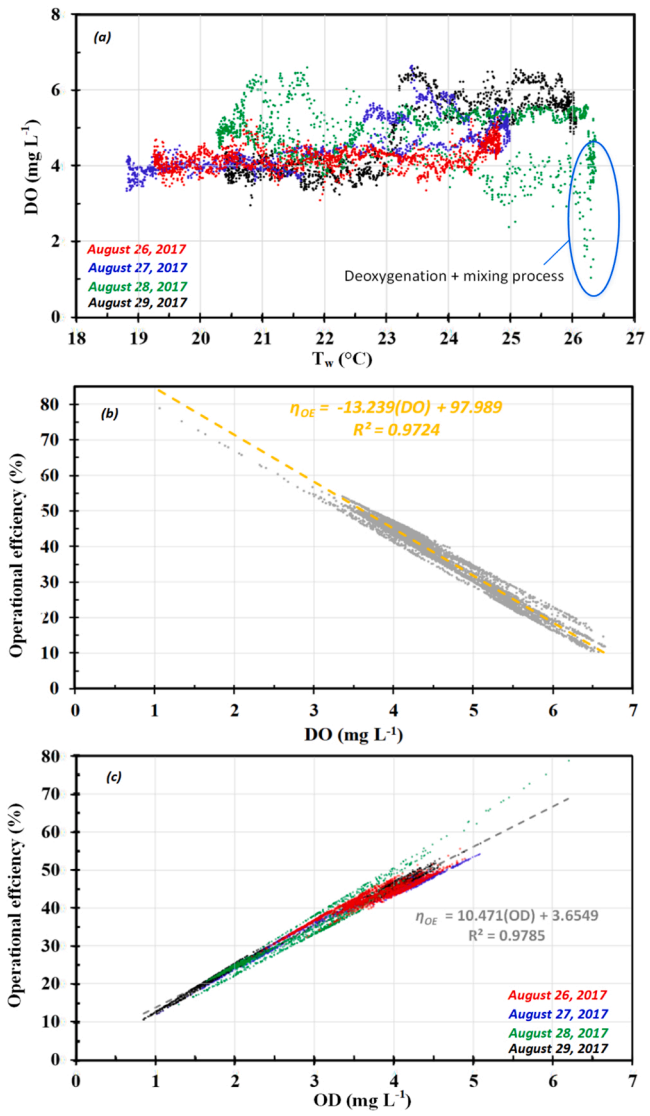


Fig. 13. Daily scatter plots of (a) DO versus water temperature, (b) operational efficiency versus dissolved oxygen (DO) for four days, and (c) operational efficiency versus oxygen deficit (OD) both daily and four days.

theoretical and experimental systematic methods. For this purpose, an experimental apparatus was made with multiple functions measuring water flow, airflow, and power consumption and monitoring real-time weather and pool dynamics flexibly.

SVAS has a different unique design and measurement capabilities the following:

- The water from the pump was carried over the main manifold, without splitting.
- The design is specific to developing the perfect vacuum and air velocity levels at the air intakes of venturi injectors.
- The design allowed us to measure the airflow rate at the inlets of each venturi without wetting of hot-wire anemometer.

During design, the following four points were considered:

(1) Water flow rate, pressure, and vacuum levels,
(2) Airflow passing from each venturi injector,
(3) Specific energy consumption per cubic meter water flow,
(4) Specific energy consumption per kg oxygen mass transfer.

Limitations of this study and implications related to theoretical, experimental, managerial, and future research are the following. The first limitation is pool data, limiting its use at different water sources. Other is assumptions on the *α-factor*, *β-factor*, and *F-factor* because of clean-tap water used in pool trials. Specifically, the author emphasizes that it would be more appropriate to use an electrical conductivity (EC) sensor for the experimental determination of the *β-factor*, considering the chemical change in water in A-F procedures. It also is pointed out that it would be appropriate to experimentally determine a mixing factor that describes the hydrodynamic mixing in water. Inspired by these studies, experiments including the development of hydrodynamic mixing index and using of EC and pH sensors have been proposed for the development of a hydrodynamic mixing index.

Experimental gains of this study are.

- design of modular-solar powered venturi aeration system,
- semi-floating prototype implementation,
- development of a systematic approach based on experiments,
- using a real-time data logging system with multiple functions.

The methodological implications:

- Development of a systematic approach based on mathematical models,
- Flow and specific power consumption characteristics,
- Determine standard and operational performance parameters.

Managerial implications:

- Monitoring of real-time weather and pool dynamics,
- Use of mathematical models for aeration,
- Understanding the mechanism of operational performance and efficiency,
- Deriving practical calculations and comparisons for available aeration efficiency equations,
- Development of a more efficient aquacultural management system,
- Developing smart aerators for aquaculture using outcomes of real-time data analytics.

Detailed research can be carried out to determine the actual amount of oxygen required in aquaculture based on physical, chemical, and biological factors. The interrelationship among these factors can be determined by considering variables such as water temperature, DO control level, diffuser depth, elevation, salinity, surface tension, mixing intensity, the concentration of solids, and basin form.

Results of this study would allow transferring to the broader fields and case studies covering different conditions. Understanding what factors took effect in a successful design and implementation process for an aerator operated in specific water basins and fishponds will be useful for academics, engineers, designers, and fish farmers. Consequently, more significant effort should be made to develop better operational strategies for aerators.

There are SVAS's two models: (1) the semi-floating prototype presented here (SVAS-I) and (2) the full-floating prototype (SVAS-II). Aeration has managed significantly more efficiently thanks to automatic control units added to these two prototypes. The experiences obtained will allow us to make a cautious extrapolation to show how changed pool conditions in future designs will affect their use. Data taken from different operating environments will provide information on the performance of the aerator at various site conditions. Real-time data collected from fishponds are crucial for programming how to operate automatic aerators. As a result, the outcomes of data analytics can be combined with a decision support tool for smart aerators. Data visualization and site-specific insights will be critical for strategic decisions. Smart aerators will operate based on real-time operational performance.

Funding

This study was funded by the Scientific and Technological Research Council of Turkey (TUBITAK-1002 Quick Support Program-Project-114O095).

Declaration of Competing Interest

The author declare that they have no known competing financial interests or personal relationships that could have appeared to influence the work reported in this paper.

Acknowledgment

I want to give thank to Yohannes Berhane Gebremedhen from Aksum University for his support during the design.

References

Afisna, L.P., Juwana, W.E., Indarto, I., Deendarlianto, D., Nugroho, F.M., 2017. Performance of porous-venturi microbubble generator for aeration process. J. Energy, Mech., Mater., Manuf. Eng. 2 (2), 73–80. https://doi.org/10.22219/JEMMME.V2I2.5054.

Applebaum, J., Mozes, D., Steiner, A., Segal, I., Barak, M., Reuss, M., Roth, P., 2001. Aeration of fish ponds by photovoltaic power. Prog. Photovolt. Res. Appl. 9, 295–301. https://doi.org/10.1016/B978-008043895-5/50027-8.

ASCE, 2007. Measurement of oxygen transfer in clean water, ASCE/EWRI 2–06: Reston, VA, 2007; 1–30. ⟨https://doi.org/10.1061/9780784408483⟩.

ASHRAE, 2009. Psychrometrics, Chapter 1, 1.1–1.16, Fundamentals (SI Edition), American Society of Heating, Refrigeration and Air Conditioning Engineers, Inc.

Bakırcı, K., 2012. General models for optimum tilt angles of solar panels: Turkey case study. Renew. Sustain. Energy Rev. 16, 6149–6159. https://doi.org/10.1016/j.rser.2012.07.009.

Baylar, A., Ozkan, F., 2006. Applications of venturi principle to water aeration systems. Environ. Fluid Mech. 6 (4), 341–357. https://doi.org/10.1007/s10652-005-5664-9.

Boyd, C.E., 1998. Pond water aeration systems. Aquacult. Eng. 18, 9–40. https://doi.org/10.1016/S0144-8609(98)00019-3.

Boyd, C.E., McNevin, A.A., 2020. Aerator energy use in shrimp farming and means for improvement. J. World Aquac. Soc. 52, 6–29. https://doi.org/10.1111/jwas.12753.

Boyd, C.E., Torrans, E.L., Tucker, C.S., 2018. Dissolved oxygen and aeration in ictalurid catfish aquaculture. J. World Aquacult Soc. 49 (1), 7–70. https://doi.org/10.1111/jwas.12469.

Boyd, C., Tucker, C., 1998. Pond Aquaculture Water Quality Management. Kluwer Academic Publishers, Massachusetts.

Boyd, C.E., 2015. Water Quality, an Introduction, second ed. Springer,, New York.

Brown, T.W., Tucker, C.S., 2014. Pumping performance of a modified commercial paddlewheel aerator for split-pond aquaculture systems. North Am. J. Aquacult 76, 72–78. https://doi.org/10.1080/15222055.2013.860067.

Brown, T.W., Tucker, C.S., Rutland, B.L., 2016. Performance evaluation of four different methods for circulating water in commercial-scale, split-pond aquaculture systems. Aquacult. Eng. 70 (1), 33–41. https://doi.org/10.1016/j.aquaeng.2015.12.002.

Campana, P.E., Wästhage, L., Nookuea, W., Tan, Y., Yan, J., 2019. Optimization and assessment of floating and floating-tracking PV systems integrated in on- and off-grid hybrid energy systems. Sol. Energy 177, 782–795. https://doi.org/10.1016/j.solener.2018.11.045.

Cancino, B., Roth, P., Reuß, M., 2004. Design of high efficiency surface aerators Part 1. Development of new rotors for surface aerators. Aquacult. Eng. 31, 83–98. https://doi.org/10.1016/j.aquaeng.2004.03.002.

Dayıoğlu, M.A., 2015. Development of a solar powered aeration system for sustainable aquaculture. Project result report. Program code: 1002, Project number: 114O095, The Scientific and Technological Research Council of Turkey (TUBITAK), Ankara.

Dong, C., Zhu, J., Wu, X., Miller, C.F., 2012. Aeration efficiency influenced by venturi aerator arrangement, liquid flow rate and depth of diffusing pipes. Environ. Technol. 33 (11), 289–1298. https://doi.org/10.1080/09593330.2011.620986.

Eltawil, M.A., Elsbaay, A.M., 2016. Utilisation of solar photovoltaic pumping for aeration systems in aquaculture ponds. Int. J. Sustain. Energy 35 (7), 629–644. https://doi.org/10.1080/14786451.2014.928295.

FAO, 2019. Fishery and Aquaculture Country Profiles - The Republic of Turkey. (Accessed 29 April 2020). ⟨http://www.fao.org/fishery/facp/TUR/en⟩.

Fujiwara, A., Okamoto, K., Hashiguchi, K., Peixinho, J., Takagi, S., Matsumoto, Y. 2007. Bubble breakup phenomena in a venturi tube. In *Fluids Engineering Division Summer Meeting*. 5th Joint ASME/JSME Fluids Engineering Conference 42886, pp. 553–560.

Gebremedhen, Y.B., 2016. Design and Construction of a Solar Powered Aeration System for Fish Farms (Ph. D. thesis). Ankara University, Graduate School of Natural and Applied Sciences.

GEPA, 2016. Solar energy potential map of Turkey. (Accessed 31 November 2016). ⟨http://www.eie.gov.tr/MyCalculator/Default.aspx⟩.

Gupta, B., Nayak, A., Kandar, K., Nair, S, T.K., 2016. Investigation of air-water two phase flow through a venturi. Exp. Therm. Fluid Sci. 70, 148–154. https://doi.org/10.1016/j.expthermflusci.2015.07.012.

Hanndel, A., Van der Lubbe, J., 2012. Handbook of biological wastewater treatment. Desing and optimization of activated sludge system. IWA Publising, London.

Huang, J., Sun, L., Liu, H., Mo, Z., Tang, J., Xie, G., Du, M., 2020. A review on bubble generation and transportation in Venturi-type bubble generators. Exp. Comput. Multiph. Flow. 2 (3), 123–134. https://doi.org/10.1007/s42757-019-0049-3.

Ioakeimidis, C., Polatidis, H., Haralambopoulos, D., 2013. Use of renewable energy in aquaculture: an energy audit case-study analysis. Glob. Nest J. 15 (3), 282–294.

Itano, T., Inagaki, T., Nakamura, C., Hashimoto, R., Negoro, N., Hyodo, J., Honda, S., 2019. Water circulation induced by mechanical aerators in a rectangular vessel for shrimp aquaculture. Aquacult. Eng. 85, 106–113. https://doi.org/10.1016/j.aquaeng.2019.03.006.

Jayraj, P., Roy, S.M., Mukherjee, C.K., Mal, B.C., 2018. Design characteristics of submersible aerator. Turk. J. Fish. Aquat. Sci. 18 (9), 1017–1023. https://doi.org/10.4194/1303-2712-v18_9_01.

Jayanthi, M., Balasubramaniam, A.A.K., Suryaprakash, S., Veerapandian, N., Ravisankar, T., Vijayan, K.K., 2021. Assessment of standard aeration efficiency of different aerators and its relation to the overall economics in shrimp culture. Aquacult. Eng. 92, 102142 https://doi.org/10.1016/j.aquaeng.2020.102142.

Jenkins, T.E., 2014. Aeration Control System Design A Practical Guide to Energy and Process Optimization. Wiley.

Jescovitch, L.N., Boyd, C.E., 2017. A case study: impacts of deviating from model research design to the commercial industry for split-pond aquaculture. Aquacult. Eng. 79, 35–41. https://doi.org/10.1016/j.aquaeng.2017.09.001.

Jiang, P., Stenstrom, M.K., 2012. Oxygen transfer parameter estimation: impact of methodology. J. Environ. Eng. 138 (2), 137–142.

Jørgensen, S.E., Bendoricchio, G., 2001. Fundamentals of Ecological Modelling. Elsevier, Amsterdam.

Kumar, A., Moulick, S., Mal, B.C., 2010. Performance evaluation of propeller-aspirator-pump aerator. Aquacult. Eng. 42, 70–74. https://doi.org/10.1016/j.aquaeng.2009.12.001.

Kumar, A., Moulick, S., Mal, B.C., 2013a. Selection of aerators for intensive aquacultural pond. Aquacult. Eng. 56, 71–78. https://doi.org/10.1016/j.aquaeng.2013.05.003.

Kumar, A., Moulick, S., Mal, B.C., 2014. Performance Evaluation of Different Aeration Systems for Aquaculture, ASABE- CSBE/SCGAB Annual International Meeting, Montreal, Quebec, July 13–16, 2014, Paper Number: 141902230, 1–12.

Kumar, A., Moulick, S., Singh, B.K., Mal, B.C., 2013b. Design characteristics of pooled circular stepped cascade aeration system. Aquacult. Eng. 56, 51–58. https://doi.org/10.1016/j.aquaeng.2013.04.004.

Lawson, B.T., 2002. Fundamentals of Aquacultural Engineering. Kluwer Academic, Massachusetts.

Lekang, O.I., 2013. Aquaculture Engineering. John Wiley & Sons, New York.

Liew, K.C.S., Rasdi, A., Budhijanto, W., Yusoff, M.H.M., Bilad, M.R., Shamsuddin, N., Nordin, N.A.H.M., Putra, Z.A., 2020. Porous venturi-orifice microbubble generator for oxygen dissolution in water. Processes 8 (10), 1266. https://doi.org/10.3390/pr8101266.

Lima, I.E., Zhu, D.Z., Rajaratnam, N., 2008. Horizontal injection of gas-liquid mixtures in a water tank. J. Hydraul. Eng. 134, 1722–1731.

Mahmudov, K., Mahmoud, A., Sur, S., Cruz, F.C., Bilton, A.M., 2019. Feasibility of a wind-powered aeration system for small-scale aquaculture in developing countries. Energy Sustain. Dev. 51, 40–49. https://doi.org/10.1016/j.esd.2019.05.003.

Moulick, S., Mal, B.C., Bandyopadhyay, S., 2002. Prediction of aeration performance of paddle wheel aerator. Aquacult. Eng. 25 (4), 217–237. https://doi.org/10.1016/S0144-8609(01)00087-5.

Mukhtar, S., Borhan, M.S., Rahman, S., Zhu, J., 2010. Evaluation of a field-scale surface aeration system in an anaerobic poultry lagoon. Appl. Eng. Agric. 26 (2), 307–318. https://doi.org/10.13031/2013.29546.

Nguyen, N.T., Matsuhashi, R., Vo, T.T.B.C., 2021. A design on sustainable hybrid energy systems by multi-objective optimization for aquaculture industry. Renew. Energy 163, 1878–1894. https://doi.org/10.1016/j.renene.2020.10.024.

Nookuea, W., Campana, P.E., Yan, J., 2016. Evaluation of solar PV and wind alternatives for self renewable energy supply: Case study of shrimp cultivation. Energy Procedia 88, 462–469. https://doi.org/10.1016/j.egypro.2016.06.026.

Park, J., Heikes, D., Recsetar, M., Roy, L.A., 2014. Performance evaluation and engineering considerations for a modular- and culvert-based paddlewheel circulator for split-ponds. Aquacult. Eng. 61, 1–8. https://doi.org/10.1016/j.aquaeng.2014.05.002.

Park, S.P., Yang, H.C., 2017. Experimental investigation on mixed jet and mass transfer characteristics of horizontal aeration process. Int. J. Heat. Mass Transf. 113, 544–555. https://doi.org/10.1016/j.ijheatmasstransfer.2017.05.120.

Peterson, E.L., Walker, M.B., 2002. Effect of speed on Taiwanese paddlewheel aeration. Aquacult. Eng. 26, 129–147. https://doi.org/10.1016/S0144-8609(02)00009-2.

Roy, S.M., Jayraj, P., Machavaram, R., Pareek, C.M., Mal, B.C., 2021. Diversified aeration facilities for effective aquaculture systems—a comprehensive review. Aquac. Int. 29, 1181–1217. https://doi.org/10.1007/s10499-021-00685-7.

Roy, S.M., Moulick, S., Mal, B.C., 2017. Design Characteristics of Spiral Aerator. J. World Aquacult Soc. 48 (6), 898–908. https://doi.org/10.1111/jwas.12410.

Roy, S.M., Moulick, S., Mukherjee, C.K., 2020. Design characteristics of perforated pooled circular stepped cascade (PPCSC) aeration system. Water Supply 20 (5), 1692–1705. https://doi.org/10.2166/ws.2020.078.

Sakamatapan, K., Mesgarpour, M., Mahian, O., Ahn, H.S., Wongwises, S., 2021. Experimental investigation of the microbubble generation using a venturi-type bubble generator. Case Stud. Therm. Eng. 27, 101238 https://doi.org/10.1016/j.csite.2021.101238.

Shelton, J.L., Boyd, C.E., 1983. Correction factors for calculating oxygen-transfer rates of pond aerators. Trans. Am. Fish. Soc. 112 (1), 120–122. https://doi.org/10.1577/1548-8659(1983)112%3C120:CFFCOR%3E2.0.CO;2.

Tchobanoglous, G., Stensel, H.D., Tsuchihashi, R., Burton, F.L., Abu-Orf, M., Bowden, G., Pfrang, W., 2014. Wastewater Engineering: Treatment and Resource Recovery, fifth ed. McGraw-Hill,, New York.

Therrien, Jean-David, Vanrolleghem, P.A., Dorea, C.C., 2019. Characterization of the performance of venturi-based aeration devices for use in wastewater treatment in low-resource settings. Water SA 45 (2), 251–258. https://doi.org/10.4314/wsa.v45i2.12.

Tukimin, A., Zuber, M., Ahmad, K.A., 2016. CFD analysis of flow through venturi tube and its discharge coefficient. IOP Conf. Ser.: Mater. Sci. Eng. 152, 012–062.

Vilaida, X., Kythavone, S., Iijima, T., 2019. Effect of Throat Size on Performance of Microbubble Generator and Waste Water Treatment. IOP Publishing,, 012031 (In IOP Conference Series: Materials Science and Engineering).

Wang, X., Shuai, Y., Zhou, X., Huang, Z., Yang, Y., Sun, J., Yang, Y., 2020. Performance comparison of swirl-venturi bubble generator and conventional venturi bubble generator. Chem. Eng. Process. -Process. Intensif. 154, 108022 https://doi.org/10.1016/j.cep.2020.108022.

Yadav, A., Kumar, A., Sarkar, S., 2020. An experimental study to evaluate the efficacy of air entrainment holes on the throat of venturi aeration system. Aquac. Int. 28, 1057–1068. https://doi.org/10.1007/s10499-020-00511-6.

Yadav, A., Kumar, A., Sarkar, S., 2021. Performance evaluation of venturi aeration system. Aquac. Eng. 93, 102156 https://doi.org/10.1016/j.aquaeng.2021.102156.

Yin, Z., Feng, Y., Wang, Y., Gao, C., Ma, N., 2018. 3-D Numerical investigation on oxygen transfer in a horizontal venturi flow with two holes. Water 10 (174), 1–13.

Yin, J., Li, J., Li, H., Liu, W., Wang, D., 2015. Experimental study on the bubble generation characteristics for a venturi type bubble generator. Int. J. Heat. Mass Transf. 91, 218–224. https://doi.org/10.1016/j.ijheatmasstransfer.2015.05.076.

Zhang, C., Song, B., Shan, J., Ni, Q., Wu, F., Wang, S., 2020. Design and optimization of a new tube aeration device. Aquac. Int. 28 (3), 985–999. https://doi.org/10.1007/s10499-020-00507-2.

Zhang, R., Sun, H., Kamthunzi, W.M., Collar, C.A., Mitloehner, F.M., 2007. Aerator performance for wastewater lagoon application. ASABE 13. International Symposium on Air Quality and Waste Management for Agriculture, Broomfield, Colorado 16–19 Sep. 2007. Publication Number 701p0907cd.

Zhu, J., Miller, J.F., Dong, C., Wu, X., Wang, L., Mukhtar, S., 2007. Aerator module development using venturi air injectors to improve aeration efficiency. Appl. Eng. Agric. 23 (5), 661–667.